FRESNEL ZONE RADIATION PATTERNS OF MICROWAVE ANTENNAS

A Thesis

Presented to

The Faculty of the Graduate Division

by

Robert Gaither Shackelford

In Partial Fulfillment

of the Requirements for the Degree

Master of Science in Electrical Engineering

Georgia Institute of Technology

June, 1962

"In presenting the dissertation as a partial fulfillment of the requirements for an advanced degree from the Georgia Institute of Technology, I agree that the Library of the Institution shall make it available for inspection and circulation in accordance with its regulations governing materials of this type. I agree that permission to copy from, or to publish from, this dissertation may be granted by the professor under whose direction it was written, or, in his absence, by the dean of the Graduate Division when such copying or publication is solely for scholarly purposes and does not involve potential financial gain. It is understood that any copying from, or publication of, this dissertation which involves potential financial gain will not be allowed without written permission.

Robert G. Shackford"

6L
12R

FRESNEL ZONE RADIATION PATTERNS OF MICROWAVE ANTENNAS

Approved:

Date Approved by Chairman: June 4, 1962

ACKNOWLEDGEMENTS

The work herein described was made possible by the use of the facilities of the Engineering Experiment Station of the Georgia Institute of Technology. I am deeply grateful for the contributions to the work made by my thesis advisor, Dr. F. Kenneth Hurd, and the enlightening criticism and encouragement given me by Dr. R. C. Johnson and Dr. M. W. Long of the Engineering Experiment Station.

TABLE OF CONTENTS

LIST OF TABLES

LIST OF ILLUSTRATIONS

SUMMARY

The purpose of this investigation was to develop a technique whereby the effects on the far zone radiation patterns of microwave antennas caused by the signal source's being in the Fresnel zone of the test antenna may be determined. To determine these effects, Fresnel zone patterns were computed for the case in which the signal source appears to be a point source when viewed from the test antenna, and also for the case in which the source has dimensions comparable to the test antenna.

It is well known that the far zone radiation pattern of an aperture antenna may be represented by a Fourier integral of the form

$$A(v) = c\int_{-a}^{a} \bar{f}(x)e^{-jvx}dx$$

where $\bar{f}(x)$ is a function of the geometry and feed pattern of the test antenna. It is shown by this study that a similar equation can be derived for the radiated field in the Fresnel zone. This equation has the form

$$A(v) = c\int_{-a}^{a} \bar{f}'(x)e^{-jvx}dx,$$

where $\bar{f}'(x)$ is not only a function of the geometry and feed pattern of the test antenna, but is also a function of the radiation pattern of the

signal source, and the separation between the signal source and the test antenna. Thus the Fresnel zone pattern may result from illumination by the Fresnel field of the signal source if the dimensions of the signal source are comparable to those of the antenna under test.

Radiation patterns were computed for a succession of points in the Fresnel and far zones for uniform, $\cos(\pi/2\ x)$, $\cos^2(\pi/2\ x)$, and experimental aperture distributions assuming point source illumination. Radiation patterns were computed at the same distances for the uniform and $\cos^2(\pi/2\ x)$ distributions assuming illumination by a large aperture transmitter. In addition to the radiation patterns, summary curves were developed showing the variation of the half power beamwidth, the first sidelobe level, and the first null depth with distance in the range $\frac{D^2}{4\lambda} \leq R < \infty$, where D is the length of the linear aperture and λ is the wavelength of the radiated field. The radiation patterns were computed by a Fourier integral analog computer which accepts the complex function $\overline{f}(x)$ or $\overline{f}'(x)$ as input data, and automatically evaluates and plots $\overline{A}(v)$ as a function of the parameter v.

The results of this study show that the Fresnel-far zone boundary is highly dependent on the aperture field distribution. The generally accepted minimum far field distance of $2D^2/\lambda$ appears to be a conservative figure for some distributions. It may be generally said that the distance to the Fresnel-far zone boundary increases as the amplitude function becomes more tapered.

It is concluded from the limited data obtained in this study that Fresnel zone patterns taken with large aperture transmitters would be extremely difficult to interpret. It is suggested that the Fresnel zone

pattern be computed by the method outlined in this thesis for each specific case in question to determine what effect the measurements will have on the far zone radiation pattern. A method is presented whereby the far zone pattern may be determined by measurements in the Fresnel zone if the aperture field distribution is known. It is felt that more work on practical illumination functions, which are not tapered to zero at the edge of the aperture, would be beneficial. An experimental program would also be useful in bearing out the applicability of the method presented in this thesis to antenna measurements. Such a program would include the comparison of calculated and measured radiation patterns for different aperture field distributions, and various size transmitting apertures.

CHAPTER I

INTRODUCTION

In the analysis of microwave antennas, the aperture field method is most commonly used (1). In this method, the antenna is represented by a planar aperture, and the radiation pattern is determined from the aperture field. The radiated field is divided into three general regions or zones called the near zone, the Fresnel zone, and the Fraunhofer or far zone. These zones are defined by their distance from the aperture surface measured in aperture diameters. Appendix I gives an exact definition of these zones; however, the following qualitative description is sufficient for an understanding of this thesis. The near zone extends from the aperture surface out to a distance of several aperture diameters. The Fraunhofer or far zone begins where the relative radiation pattern is no longer dependent upon the distance to the point of observation, and extends to infinity. The Fresnel zone is situated between the near and far zones. The definitions applied to these zones are somewhat arbitrary, and hence the boundaries between the zones are not sharply defined.

Since most antennas are designed to operate in the far zone, where the radiated field may be represented locally by a plane wave, most measurements are made in this region. Microwave antennas are commonly described by their far field radiation patterns.

If the medium through which the field is transmitted is linear, passive, and isotropic, the reciprocity theorem may be applied, and the

transmitting and receiving patterns are the same. In practice, the far zone radiation pattern of an antenna is usually determined by operating the antenna under test as a receiving antenna. The test antenna is rotated about a vertical axis in a field which is uniform in phase and amplitude over the aperture surface when the test antenna is "looking" directly at the transmitting source. This "illumination" may be approximated by a point source having an isotropic field pattern provided the separation between the point source and the antenna is sufficiently large. As the point source is moved in toward the aperture, the phase deviation across the aperture becomes significant, and the Fresnel zone pattern is obtained.

When attempting to measure the radiation pattern of an antenna, a decision must be made by the engineer as to what distance or range constitutes the far zone. A rule which is often applied is that the test antenna should be at least $2\ D^2/\lambda$ distance from the point at which the transmitter is placed, where D is the largest linear dimension over the aperture, and λ is the wavelength in free space. At this distance, the maximum phase deviation is $\pi/8$ radians for a point source.

A large class of microwave antennas is of the narrow-beam wide-aperture type, and often their $2\ D^2/\lambda$ distance is prohibitively large. Methods do exist (2) whereby arrays may be focused in a manner which allows one to make pattern measurements at a convenient distance; however, this method is not applicable to antennas which have rigid reflectors. A good antenna test range requires that the transmitter and receiver locations be elevated and separated by an obstacle-free path.

Since most antenna test ranges usually have the distance between the transmitter and receiver sites fixed, in many cases the available range is less than the theoretical $2\ D^2/\lambda$ far field distance. An understanding of the behavior of the field in the transition region between the Fresnel and far zone would in many cases allow the engineer to use range distances less than the theoretical far zone range of $2\ D^2/\lambda$ without sacrificing the information desired from the radiation pattern.

The theoretical $2\ D^2/\lambda$ range distance is based upon approximations which are valid only if the transmitter appears to be a point source when viewed from the receiving position. This is equivalent to saying that the test antenna is in the far zone of the transmitter. Since most antenna pattern ranges are far from ideal, a narrow-beam wide-aperture source is usually used as a transmitter to minimize reflections, and to obtain the necessary gain. As the separation between the transmitter and receiver is shortened, the receiving antenna may be in the Fresnel zone of the transmitter. In order to make use of the shorter ranges, it may then be necessary to interpret the data obtained from the Fresnel zone receiving pattern of one antenna receiving energy from the Fresnel zone of the transmitting antenna.

There have been numerous papers (3),(4),(5) in the last few years concerning the problem of antenna measurements in the near and Fresnel zones. Some have attempted to better define the boundary regions. Others have dealt with the use of the scalar integral approximations to the exact integrals representing the field radiated from a plane aperture. Still others have considered the transfer of power between antennas in the Fresnel zone. None of these works, however, have examined the case

in which the antenna under test is being illuminated by the Fresnel pattern of the transmitting source. Some interesting conclusions can be drawn from each paper. However, the conclusions vary from paper to paper due to their dependence on antenna dimensions and energy distribution across the aperture. One of the most recent works, by R. C. Hansen and L. L. Bailin (3), examined the scalar integral approximation (or Fresnel approximation) to determine the region in which this approximation is valid. Hansen and Bailin's paper also attempted to define the boundary between the Fresnel and far fields on the basis of axial power density. The exact integral equations for a plane aperture were solved numerically and the axial power density plotted as a function of distance from the aperture surface. Some of the important conclusions drawn by Hansen and Bailin are listed below:

1. The axial power density varies as $1/R^2$ from infinity down to a distance $R = D^2/\lambda$ for all aperture distributions. Based on this result, D^2/λ seems to be a good point for the transition between the Fresnel and far zones. (Since this definition is based on axial power density, the far field region so defined is not necessarily the region in which the radiation pattern is independent of the distance to the point of observation as defined in the first paragraph of Chapter I. It will be shown in this thesis that the variation of radiation pattern parameters in the region $D^2/\lambda < R < 2\ D^2/\lambda$ depends greatly on the aperture energy distribution.)

2. The Fresnel approximations are useful from $R = D^2/\lambda$ to a distance of several aperture diameters for large aperture antennas. The

minimum distance increases for smaller apertures. It must be said, however, that the small angle approximations give poor results at wide angles in this region.

3. A general trend has been noted in the deterioration of the radiation patterns independent of antenna dimensions and aperture energy functions.

The object of this study is to develop a technique whereby the effects on the far zone radiation pattern of microwave antennas caused by the signal source's being in the Fresnel zone of the test antenna may be determined. The first condition to be examined will be the case where the signal source appears to be a point source. The second condition to be examined will be the case where the source has dimensions comparable to the test antenna thus examining the condition where the test antenna is in the Fresnel zone of the signal source. It will be shown that the rather difficult equations representing the radiation patterns of microwave antennas under these conditions may be reduced to a Fourier integral form which is easily solved by a commercially available computer. A typical problem will be solved, using four different aperture field distributions, to illustrate the technique, and to indicate the general features of the result.

It will be shown in Appendix II that the far zone radiation pattern of a narrow-beam microwave antenna may be represented by

$$A(v) = c\int_{-a}^{a} \bar{f}(x)e^{-jvx}dx \qquad (1)$$

where $\bar{f}(x)$ is a function of the geometry and feed pattern of the test antenna. A Fourier integral computer which accepts the complex function $\bar{f}(x)$ as input data, and computes the integral $A(v)$ as a function of the parameter v is discussed in Appendix III.

It will be shown in Chapter II that an equation similar to the far zone relation may be derived for the Fresnel zone. This equation has the form

$$A(v) = c \int_{-a}^{a} \bar{f}'(x) e^{-jvx} dx \qquad (2)$$

where the complex function $\bar{f}'(x)$ is not only a function of the geometry and feed pattern of the test antenna, but also a function of the radiation pattern of the signal source and the separation between the signal source and the antenna under test. The complex functions $\bar{f}(x)$ and $\bar{f}'(x)$ are called aperture field distributions, and describe the amplitude and phase of the field across the aperture of the test antenna.

Four antenna field distributions are presented in Chapter III, for the case in which the signal source appears as a point source when viewed from the test antenna. In the same chapter, two of these distribution functions are examined for the case in which the signal source has dimensions comparable to the test antenna. Curves are presented for the amplitude and phase functions across the aperture showing their dependence upon the radiation pattern of the signal source at successive points in the Fresnel and far zones.

Radiation patterns are presented in Chapter IV for each of the six conditions described in Chapter III. Summary curves of several of the radiation pattern characteristics are included to illustrate their variation with separation between the signal source and the test antenna.

CHAPTER II

PROCEDURE

Field Equations for Point Source Illumination.--The approach to the problem begins with an examination of the integral equations which yield the electromagnetic field at a point P in the right hemisphere, due to diffraction through a large plane aperture of arbitrary shape and size situated in the x-y plane (see Figure 1). If we neglect the line integrals around the edge of the aperture, the scalar field equation as given by Silver (6) is

$$A(\theta,\phi) = \frac{1}{4\pi}\int_S \bar{F}(x,y)\,\frac{e^{-jkr}}{r}\left[\,(jK+\frac{1}{r})\overline{i_z}\cdot\bar{r} + jK\overline{i_z}\cdot\bar{s}\,\right]dxdy, \quad (3)$$

where

$\bar{F}(x,y) = F(x,y)e^{j\psi(x,y)}$ is a phasor which gives the amplitude and phase of the field over the surface of the aperture,

λ is the wavelength of the radiated field,

K is $2\pi/\lambda$,

$\bar{s}$, $\overline{i_z}$, $\bar{r}$ are unit vectors, $\bar{s}$ being a unit vector in the direction of power flow at the aperture surface, and $\overline{i_z}$ and $\bar{r}$ are unit vectors defined in Figure 1.

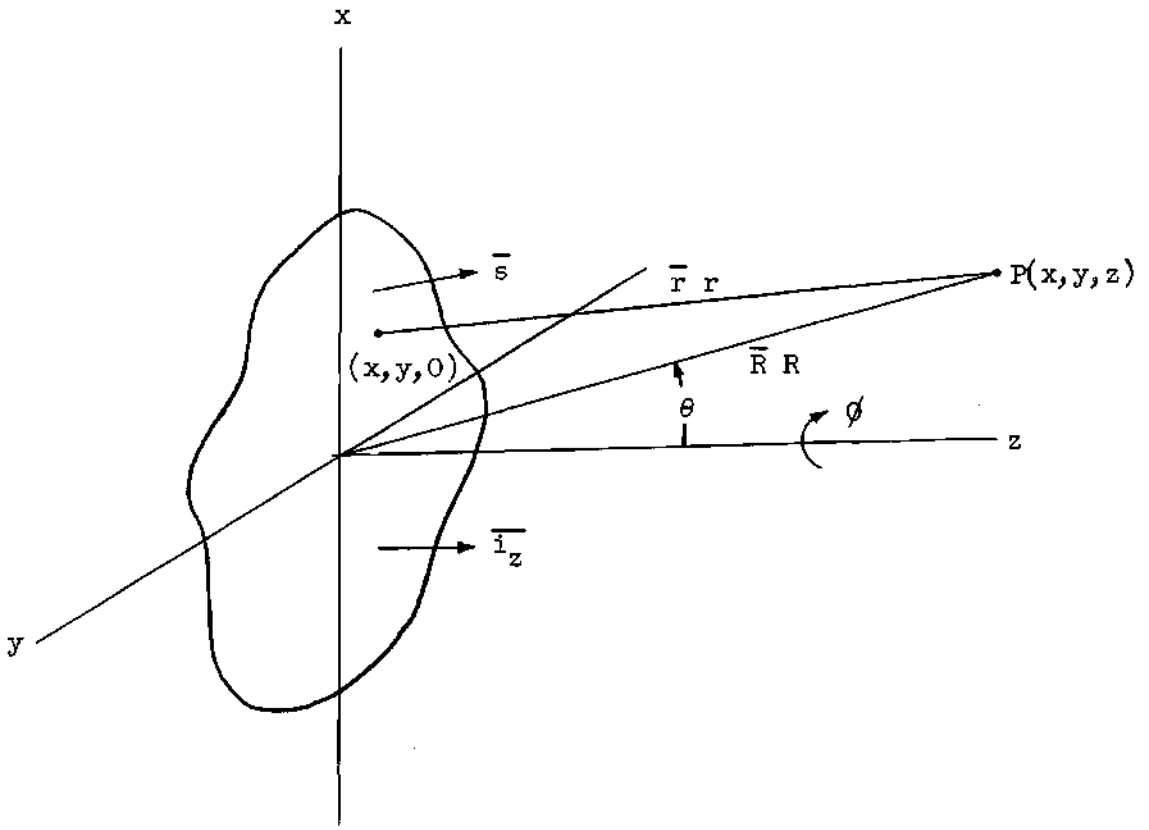

Figure 1. Aperture and Diffraction Field Geometry

If we restrict the points P to lie in the x-z plane at a constant radius R, ($R \geq 2D^2/\lambda$) it is shown in Appendix II that the narrow beam far field equation may be written as

$$A(\theta) = c\int_{-a}^{a} \bar{f}(x)e^{-jK\sin\theta x}dx \ . \qquad (4)$$

The function $\bar{f}(x) = f(x)e^{j\Psi(x)}$ is the aperture field distribution, and for reflector type antennas depends on the geometry of the antenna and the radiation pattern of the feed. Since the feed is usually placed at the focus of the reflector, $e^{j\Psi(x)}$ is usually constant, and $\bar{f}(x) = f(x)$. Equation 4 is valid in the far zone ($\frac{2D^2}{\lambda} \leq R < \infty$), and may be recognized as a Fourier integral which is readily solved if the complex aperture field function $\bar{f}(x)$ is known.

As the point of observation is moved in toward the aperture surface, the approximations used in the phase term e^{-jKr} of Equation 3 are no longer valid, and it is shown in Appendix II that Equation 3 becomes

$$A(\theta) = c\int_{-a}^{a} \bar{f}(x)e^{-j[K\sin\theta x - Kx^2/2R]}\,dx \ . \qquad (5)$$

This equation is valid in the range of R which satisfies the approximations given in Appendix II; however, it may be generally said that Equation 5 is a good approximation of the radiated field with negligible error for a minimum range of $R_{min} = 1/4\ D^2/\lambda$. It must be remembered that Equations 4 and 5, and the derivations that follow, are valid only if

the antenna meets the conditions described in Appendix II. These equations are not valid for antennas with broad radiation patterns or with excessive phase error across the aperture, although they are often indiscriminately used in both cases. This is not as prohibitive as it may sound at first reading since a large class of microwave antennas do meet these conditions.

A comparison of Equations 4 and 5 shows that Equation 5 could also represent the electric field at a point P in the far zone resulting from an aperture with a quadratic phase deviation of $Kx^2/2R$. It will be shown in Chapter III that this is the approximate phase error across the aperture due to illumination by a point source (with an isotropic field pattern) placed on the z-axis a distance R from the aperture surface (see Figure 2).

Calculation of the Radiation Pattern.--There exists a Fourier integral computer (described in Appendix III) which computes the integral

$$I(u) = \int_{-1}^{1} \overline{P}(x) e^{jux} dx \ , \qquad (6)$$

and plots the result on a rectangular pattern recorder as a function of the parameter u. The complex function $\overline{P}(x)$ is inserted as data, and the output I(u) is plotted either linearly or logarithymically as a function of u. If the aperture field distribution $\overline{f}(x)$ is known, the radiation pattern of the antenna is easily determined. For example, if one wished to compute the radiation pattern of an antenna which had an aperture

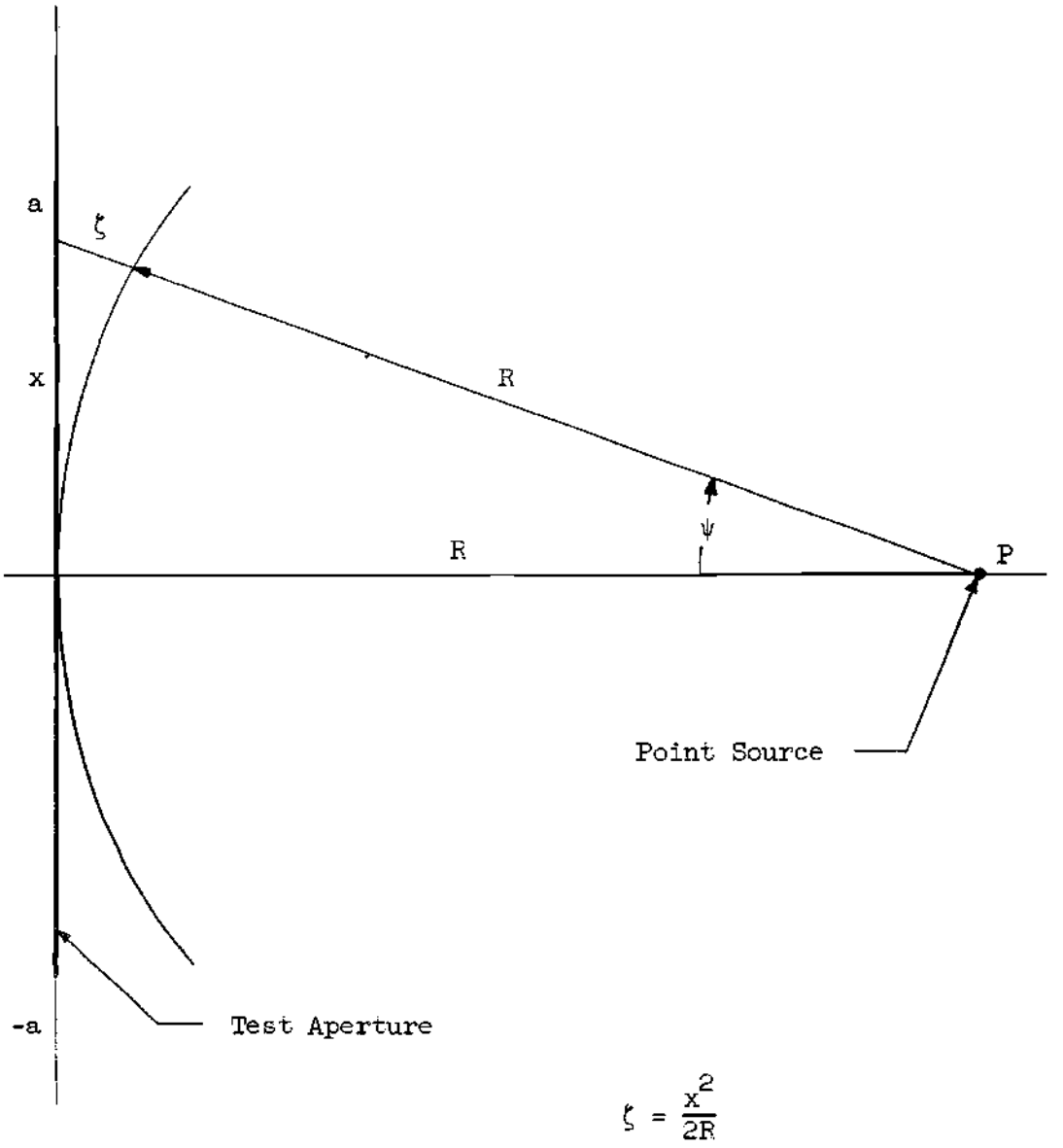

Figure 2. Phase Error over the Aperture for Point Source Illumination

field function $\bar{f}(x) = \cos\left(\frac{\pi}{2}x\right)$, $-1 \leq x \leq 1$, at a range $R = D^2/2\lambda$, then Equation 5 would become

$$A(\theta) = c\int_{-a}^{a} \cos\left(\frac{\pi}{2}\frac{x}{a}\right)e^{-jK\left[x\sin\theta - \frac{x^2}{D^2/\lambda}\right]}dx\,, \qquad (7)$$

and by normalizing the variable of integration and setting $a = D/2$,

$$A(\theta) = \frac{Dc}{2}\int_{-1}^{1} \cos\left(\frac{\pi}{2}x\right)e^{j\left[\frac{\pi x^2}{2} - \frac{KDx\sin\theta}{2}\right]}dx \qquad (8)$$

If Equation 8 is compared with Equation 6, it is obvious that the computer input function $\bar{P}(x) = \cos\left(\frac{\pi}{2}x\right)e^{j\pi x^2/2}$, $-1 \leq x \leq 1$, and that the parameter $u = \frac{KD\sin\theta}{2}$.

Field Equations Adapted to a Large Aperture Transmitter.--In practice, the transmitter radiation pattern is not isotropic for reasons given in Chapter I, and as the separation between the transmitting source and test antenna is decreased, it is quite possible that the test antenna may be in the Fresnel field of the transmitting antenna.

If we replace the point source at P by a large aperture transmitter, each point along the cylindrical wavefront in Figure 3 will have a magnitude and phase which is a function of the angle ψ. Let the magnitude and phase functions be $F(\psi)$ and $G(\psi)$, respectively. For the small values of ψ used in the Fresnel approximation, the magnitude along the x-axis due to the illuminating wavefront can be represented by

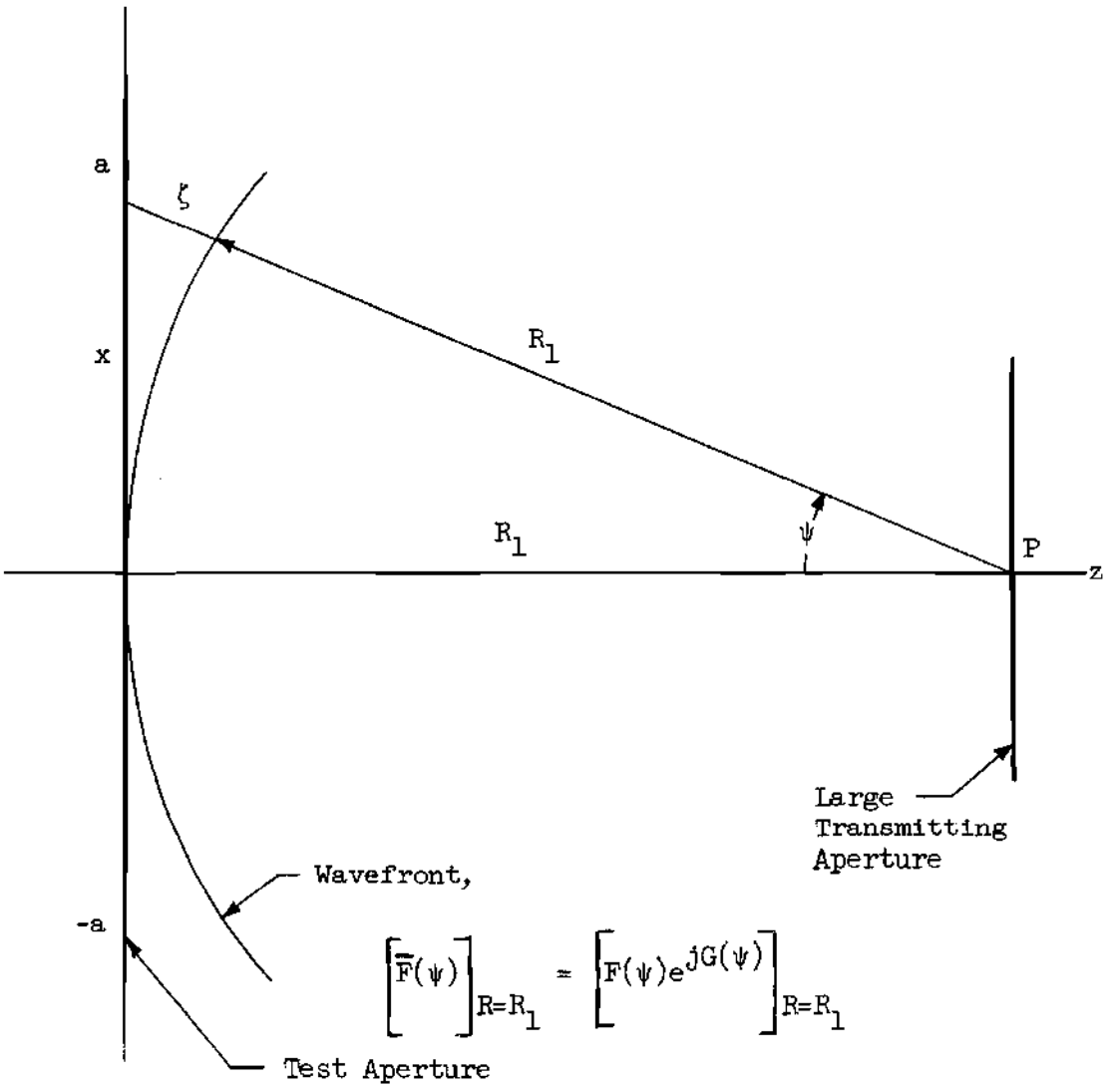

Figure 3. Aperture Distribution Due to Large Aperture Transmitter

$$f(x) = \frac{F(\psi)}{[\cos(\psi)]^{1/2}} \cdot \tag{9}$$

Therefore, if an aperture having a field distribution given by

$$\tilde{f}(x) = f(x)\, e^{j\Psi(x)}$$

is illuminated by a large aperture transmitter, the equivalent aperture field function is

$$\bar{F}(x) = \frac{F(\psi)}{[\cos(\psi)]^{1/2}} f(x)\, e^{j[\Psi(x) + G(\psi)]} \cdot \tag{10}$$

Equation 3 may then be written

$$A(\theta) = c \int_{-a}^{a} \frac{F(\psi) f(x)}{[\cos(\psi)]^{1/2}}\, e^{-j[K\sin\theta x - K\frac{x^2}{2R} - \Psi(x) - G(\psi)]} dx \cdot \tag{11}$$

We may then cast Equation 7 into computer form by writing

$$A(\theta) = C \int_{-1}^{1} \frac{F(\psi) f(ax)}{[\cos(\psi)]^{1/2}}\, e^{j[\Psi(ax)+G(\psi)+K\frac{(ax)^2}{2R}]} e^{-jKax\sin\theta} dx \cdot \tag{12}$$

Hence the parameters of Equation 6 are

$$\bar{P}(x) = \frac{F(\psi)\, F(x)}{[\cos(\psi)]^{1/2}}\, e^{j[\Psi(ax) + G(\psi) + K\frac{(ax)^2}{2R}]}, \tag{13}$$

where $F(x) = f(ax)$,

where $\psi = \tan^{-1}\left(\frac{ax}{R}\right)$,

and $u = Ka\sin\theta$.

Note that the constant c in Equation 12 is a scale factor and is arbitrarily set equal to one in Equation 6.

Steps to the Solution of the General Problem.--Equations 5 and 12 are the basic equations which will be used in the solution of the problem outlined in this thesis. A general outline of the steps used in the interpretation of the Fresnel zone patterns of a test antenna being illuminated by a transmitting antenna, whose dimensions are comparable to those of the test antenna, are listed below:

1. Assuming point source illumination, radiation patterns are computed using Equation 5 for a succession of points in the Fresnel and far zones of the test antenna.

2. Next the complex field of the actual transmitter, with a finite aperture, is determined at the same values of R used in step No. 1. Equation 5 is used, and the amplitude and phase are plotted against the polar angle ψ.

3. From the radiation patterns determined in step No. 2, the functions $F(\psi)$ and $G(\psi)$ pertinent to Equation 12 are plotted.

4. The complex field of the test antenna is then calculated from Equation 12 at the preselected values of R.

5. The results of steps No. 1 and No. 4 will then be compared to interpret the use of a large aperture transmitter in the determination of Fresnel zone radiation patterns.

CHAPTER III

APPLICATION OF THE METHOD IN THE COMPUTATION OF RADIATION PATTERNS FOR TWO CASES

Aperture Functions for Point Source Illumination-Case I.--It was shown in Chapter II that the aperture function necessary for the solution of Equation (6) is given by

$$\overline{P}(x) = \frac{F(x)F(\psi)}{[\cos(\psi)]^{1/2}} e^{j[\Psi(ax) + G(\psi) + K\frac{(ax)^2}{2R}]} . \qquad (14)$$

The first step in obtaining the radiation pattern of an antenna then becomes one of determining the aperture function as given in Equation (14) for a given set of conditions.

Consider a linear aperture of length D being illuminated by an isotropic radiator placed at a point p on the z-axis R distance from the aperture surface (see Figure 2). Since the amplitude of the wavefront is uniform over the aperture surface, the aperture amplitude function $Re[\overline{P}(x)]$ is dependent only on the geometry of the reflector, and the radiation pattern of the feed. The amplitude function for point source illumination is

$$Re[\overline{P}(x)] = F(x) . \qquad (15)$$

The phase deviation ζ at any point along the aperture surface (see Figure 2) is given by

$$(R + \zeta) = (R^2 + x^2)^{1/2} , \tag{16}$$

where $(R^2 + x^2)^{1/2} = R + \frac{1}{2} x^2/R - \frac{1}{8} x^4/R^3 + \ldots .$ for $R^2 > x^2$. If $R^2 \gg x^2$, then

$$(R^2 + x^2)^{1/2} \approx R + \frac{1}{2} x^2/R , \tag{17}$$

and

$$\zeta \approx \frac{1}{2} x^2/R . \tag{18}$$

The phase function for the case of point source illumination may then be written

$$\mathrm{Im}[\overline{P}(x)] = e^{j[\frac{(ax)^2}{2R} + \psi(ax)]} . \tag{19}$$

The term $\psi(ax) = \mathrm{Im}[\overline{F}(x)]$ is usually zero as was pointed out in Chapter II, and Equation 19 becomes

$$\mathrm{Im}[\overline{P}(x)] = e^{j \frac{(ax)^2}{2R}} . \tag{20}$$

The complex aperture function for the case of point source illumination is

$$\overline{P}(x) = F(x) e^{j \frac{(ax)^2}{2R}} . \tag{21}$$

The amplitude function $F(x)$ depends only on the antenna under test and is constant with range; however, the phase term $(ax)^2/2R$ must be evaluated at each range R at which the radiation pattern is to be computed.

The radiation patterns for four different amplitude functions are presented in Chapter IV. These functions are:

Case Ia . . . . $Fa(x)$ = uniform illumination

Case Ib . . . . $Fb(x) = \cos(\pi/2\ x)$, $-1 \leq x \leq 1$

Case Ic . . . . $Fc(x) = \cos^2(\pi/2\ x)$, $-1 \leq x \leq 1$

Case Id . . . . $Fd(x)$ = experimental illumination function

These four functions are illustrated in Figure 4. The radiation patterns were computed for an aperture width of $D = 50\lambda$. The complex radiation field $\bar{A}(\theta)$ for each of these four cases will be denoted as follows:

Case Ia . . . . $\bar{A}_{Ia}(\theta)$

Case Ib . . . . $\bar{A}_{Ib}(\theta)$

Case Ic . . . . $\bar{A}_{Ic}(\theta)$

Case Id . . . . $\bar{A}_{Id}(\theta)$

The radiation pattern is given in Chapter IV for all four cases; in addition, the phase pattern ($\text{Im}\ \bar{A}(\theta)$) is presented for cases Ia and Ic for use in the computation of the radiation patterns in Case II.

Aperture Functions for Illumination by a Large Aperture Transmitter-Case II.--When the point source is replaced by a large aperture transmitter, the aperture function $\bar{P}(x)$ becomes a function of the radiation pattern of the transmitter and the separation between the transmitter and the test aperture as given by Equation 14. In Case II, radiation patterns will be computed for the condition in which the test antenna

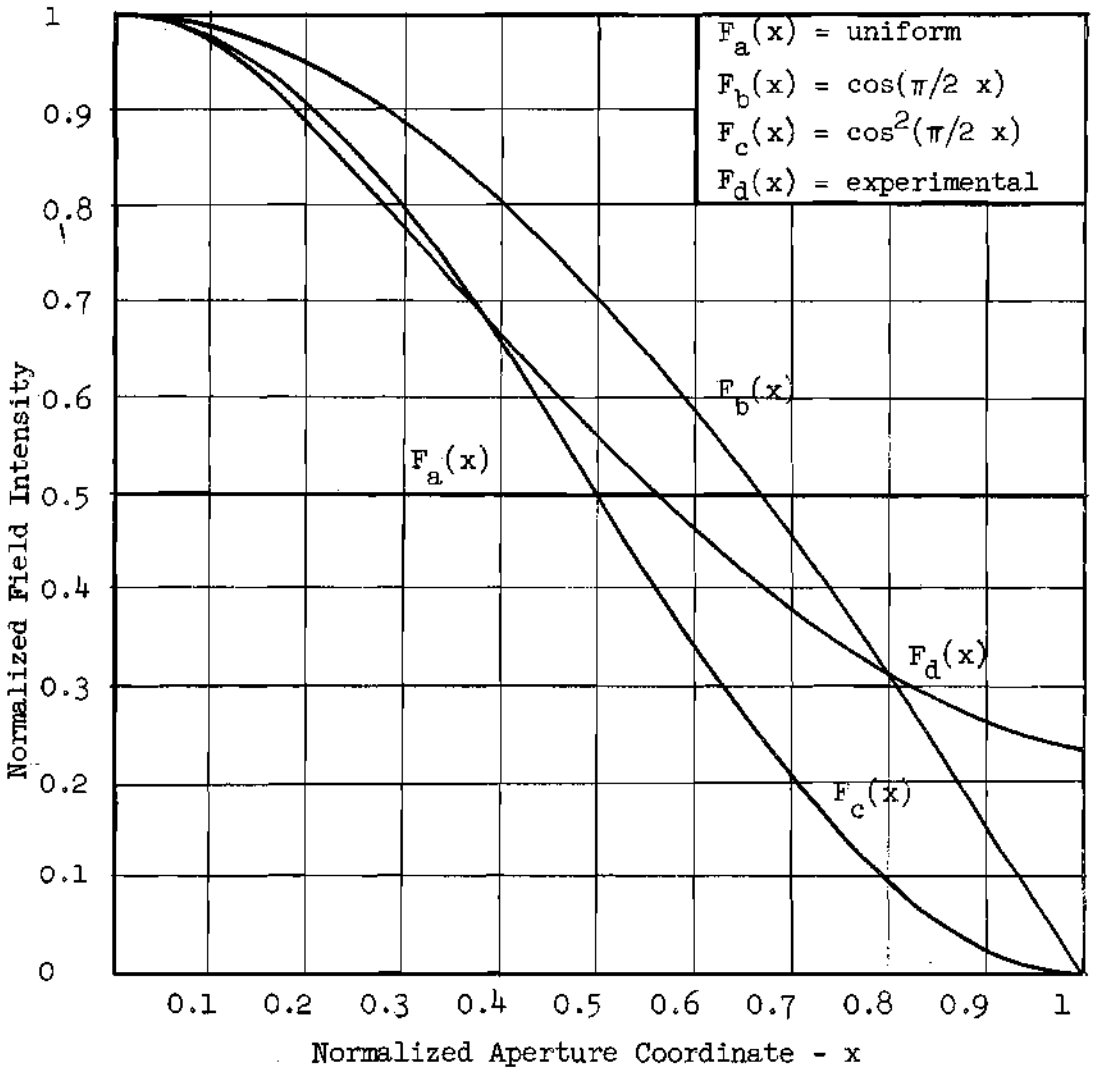

Figure 4. Aperture Amplitude Distributions Over One Half the Aperture for Case I

is illuminated by a transmitting antenna having the same aperture width and amplitude function F(x). An aperture width D = 50λ will be used so that the results may be compared with those of Case I. The uniform and $\cos^2(\frac{\pi}{2}x)$ distributions were chosen for Case II. These will be designated as

$$\text{Case IIa} \ldots . \ Fa(x) = \text{uniform illumination}$$

$$\text{Case IIc} \ldots . \ Fc(x) = \cos^2(\tfrac{\pi}{2}x) \quad -1 \leq x \leq 1$$

The aperture functions necessary for the computation of radiation patterns for these two cases are

$$\bar{P}_{IIa}(x) = \frac{F_a(x)F_a(\psi)}{[\cos(\psi)]^{1/2}} e^{j[K\frac{(ax)^2}{2R} + \Psi_a(ax) + G_a(\psi)]}, \qquad (22)$$

and

$$\bar{P}_{IIc}(x) = \frac{F_c(x)F_c(\psi)}{[\cos(\psi)]^{1/2}} e^{j\,K\frac{(ax)^2}{2R} + \Psi_c(ax) + G_c(\psi)}, \qquad (23)$$

where $\psi = \tan^{-1} x/R$.

Referring back to the steps in the solution of the general problem as outlined in Chapter II we see that steps 1 and 2 have been completed in the computations of the complex radiation patterns for Case I. From Figure 3, step 3 may be accomplished by recognizing that

$$\left[F_a(\psi)\right]_{R=R_1} = \text{Re}\left[\bar{A}_{Ia}(\theta)\right]_{R=R_1}, \qquad (24)$$

where $\psi = \theta = \tan^{-1}(x/R_1)$,

and

$$\left[G_a(\psi)\right]_{R=R_1} = \mathrm{Im}\left[\bar{A}_{Ia}(\theta)\right]_{R=R_1} . \tag{25}$$

In a similar manner,

$$\left[F_c(\psi)\right]_{R=R_1} = \mathrm{Re}\left[\bar{A}_{Ic}(\theta)\right]_{R=R_1} , \tag{26}$$

where $\psi = \theta = \tan^{-1}(x/R_1)$,

and

$$\left[G_c(\psi)\right]_{R=R_1} = \mathrm{Im}\left[\bar{A}_{Ic}(\theta)\right]_{R=R_1} . \tag{27}$$

At each value of distance R_n for which the radiation pattern is to be computed, the functions $\bar{A}_{Ia}(\tan^{-1} x/R_n)$ and $\bar{A}_{Ic}(\tan^{-1} x/R_n)$ are determined for $-D/2 \leq x \leq D/2$.

The aperture functions $\mathrm{Re}[\bar{P}_{IIa}(x)]$, $\mathrm{Im}[\bar{P}_{IIa}(x)]$, $\mathrm{Re}[\bar{P}_{IIc}(x)]$, and $\mathrm{Im}[\bar{P}_{IIc}(x)]$ are shown in Figures 5, 6, 7, and 8, respectively, for a succession of points in the Fresnel and far zones, once again assuming that $\Psi_a(x) = \Psi_c(x) = 0$. The radiation patterns $\mathrm{Re}[\bar{A}_{IIa}(\theta)]$ and $\mathrm{Re}(\bar{A}_{IIc}(\theta)]$ computed for cases IIa and IIc are shown in Chapter IV.

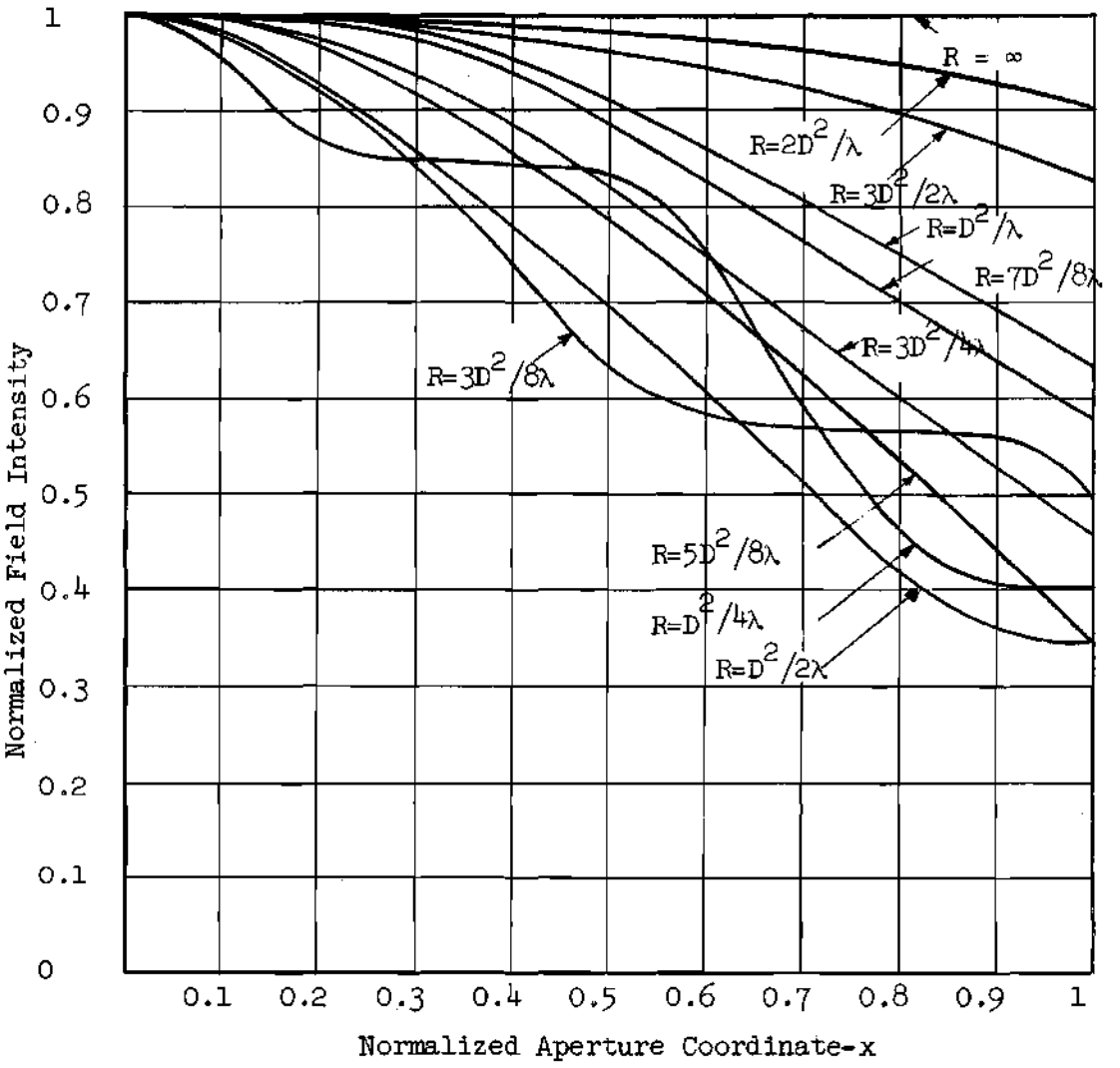

Figure 5. Aperture Amplitude Distributions Over One Half the Aperture for Case IIa

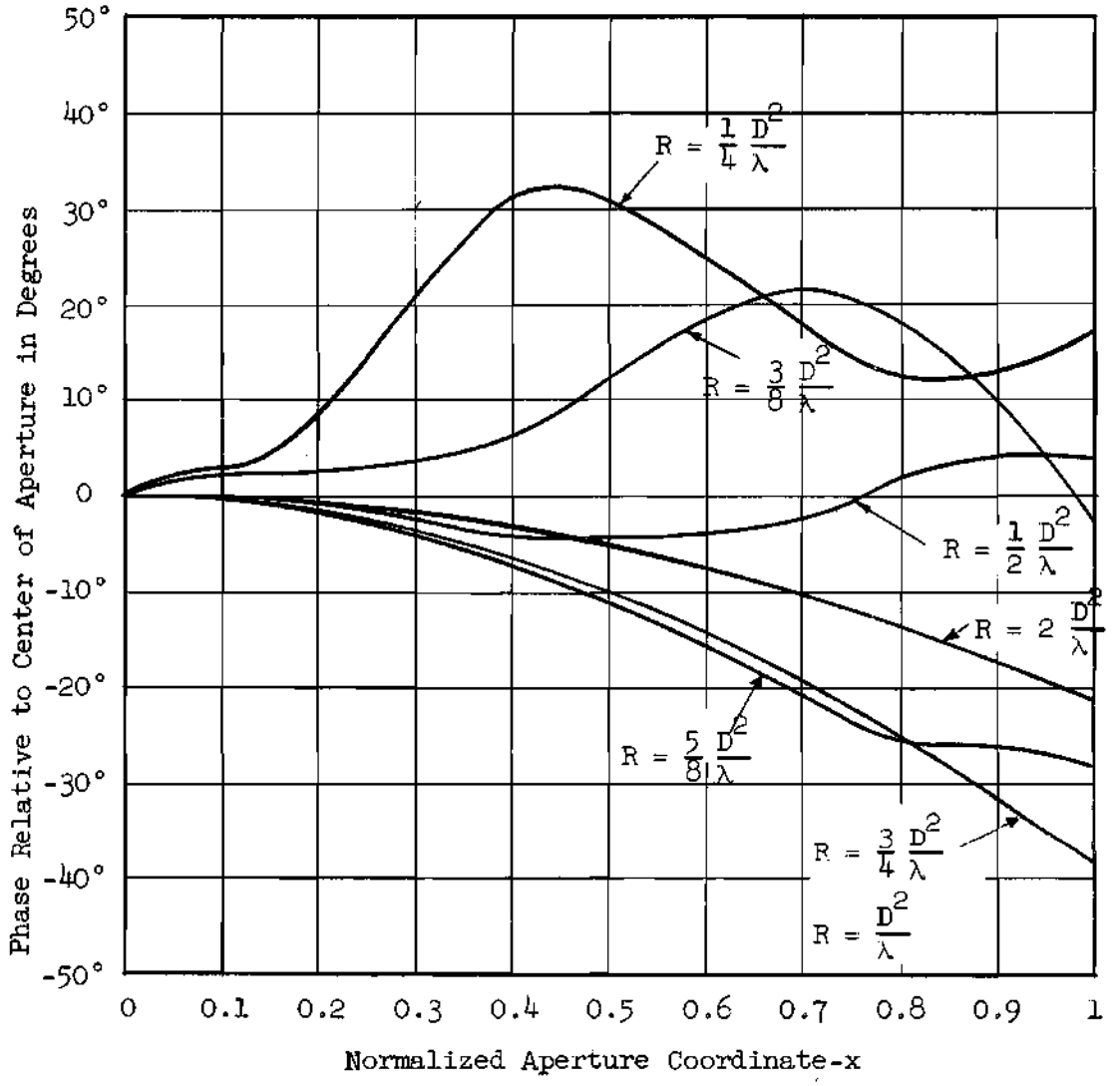

Figure 6. Aperture Phase Distributions Over One Half the Aperture for Case IIa

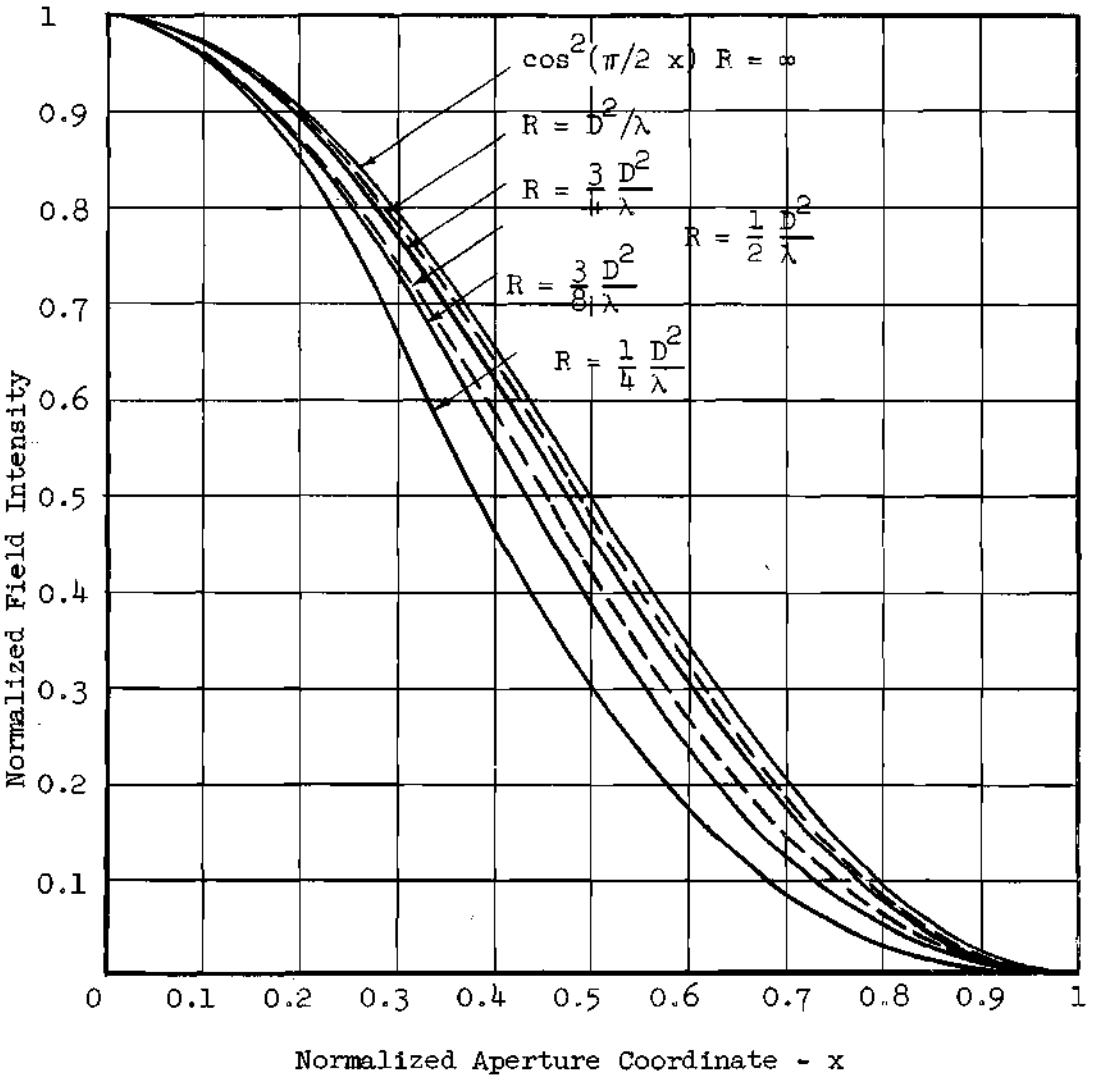

Figure 7. Aperture Amplitude Distributions Over One Half the Aperture for Case IIc

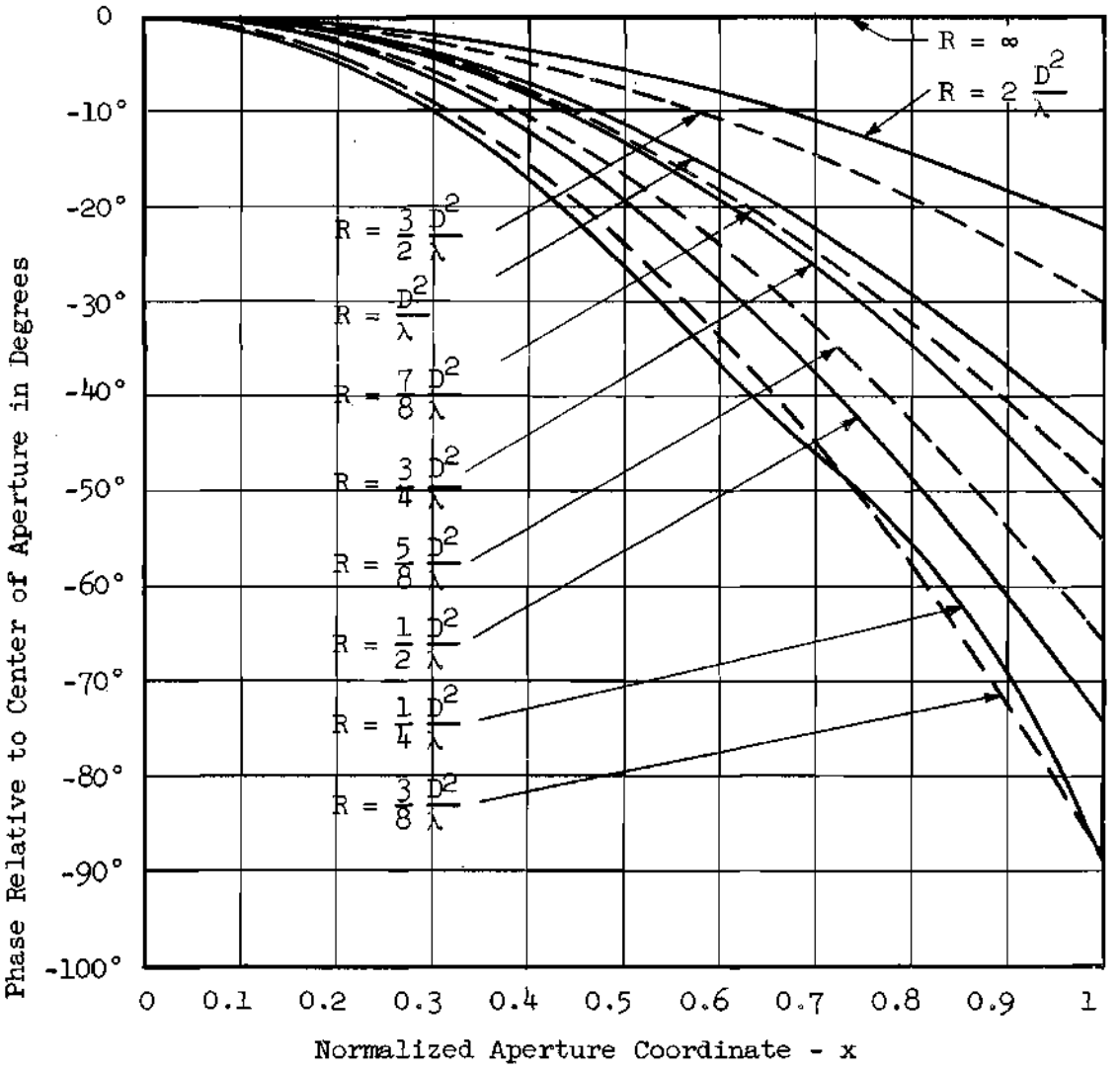

Figure 8. Aperture Phase Distributions Over One Half the Aperture for Case IIc

CHAPTER IV

RESULTS

The radiation patterns for Case I are shown in Figures 9 through 12 for a succession of points in the range $1/4\ D^2/\lambda \leq R < \infty$. Figures 13 and 14 show the phase variation in the same range of R for Cases Ia and Ic. The radiation patterns for Case II are shown in Figures 15 and 16. Figures 17, 18, and 19 show the variation of the radiation pattern characteristics as a function of distance for each of the aperture distributions in Cases I and II. The accuracy of the results is discussed in Appendix III, which describes the computer used in the calculation of the radiation patterns. The radiation patterns shown in Figures 9-16 are all normalized to their peak value of field intensity at $\theta = 0$.

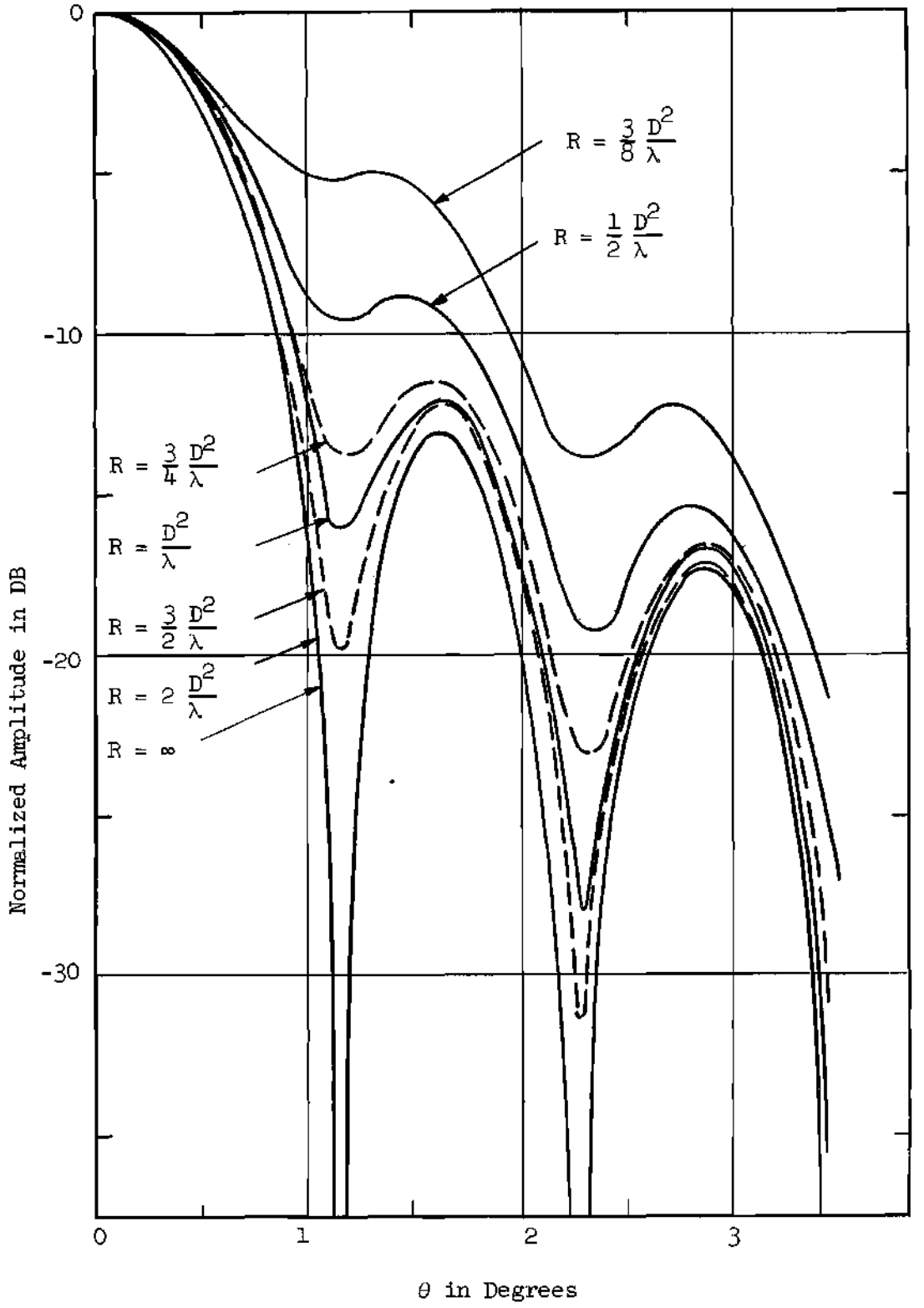

Figure 9. Radiation Patterns for Case Ia

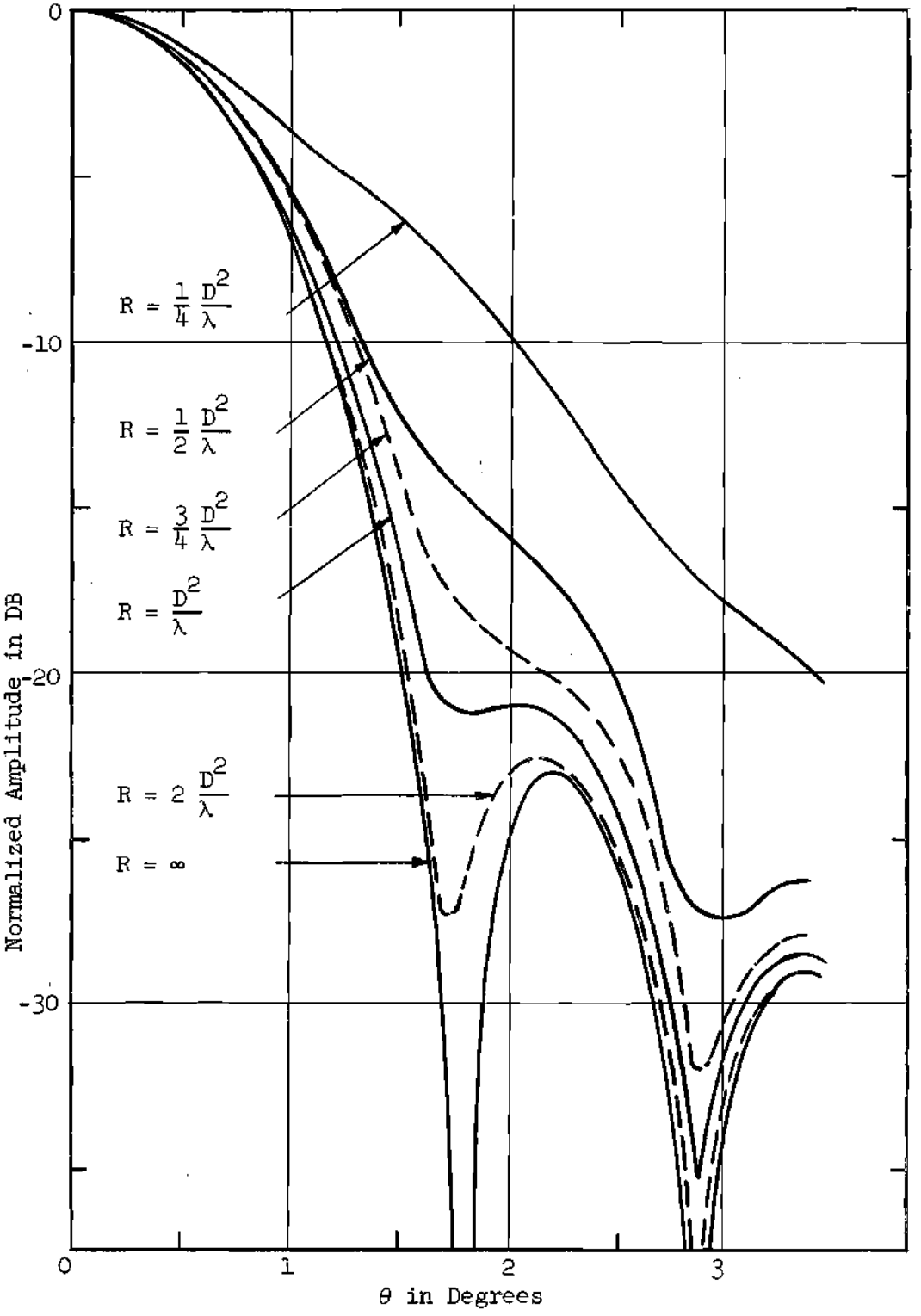

Figure 10. Radiation Patterns for Case Ib

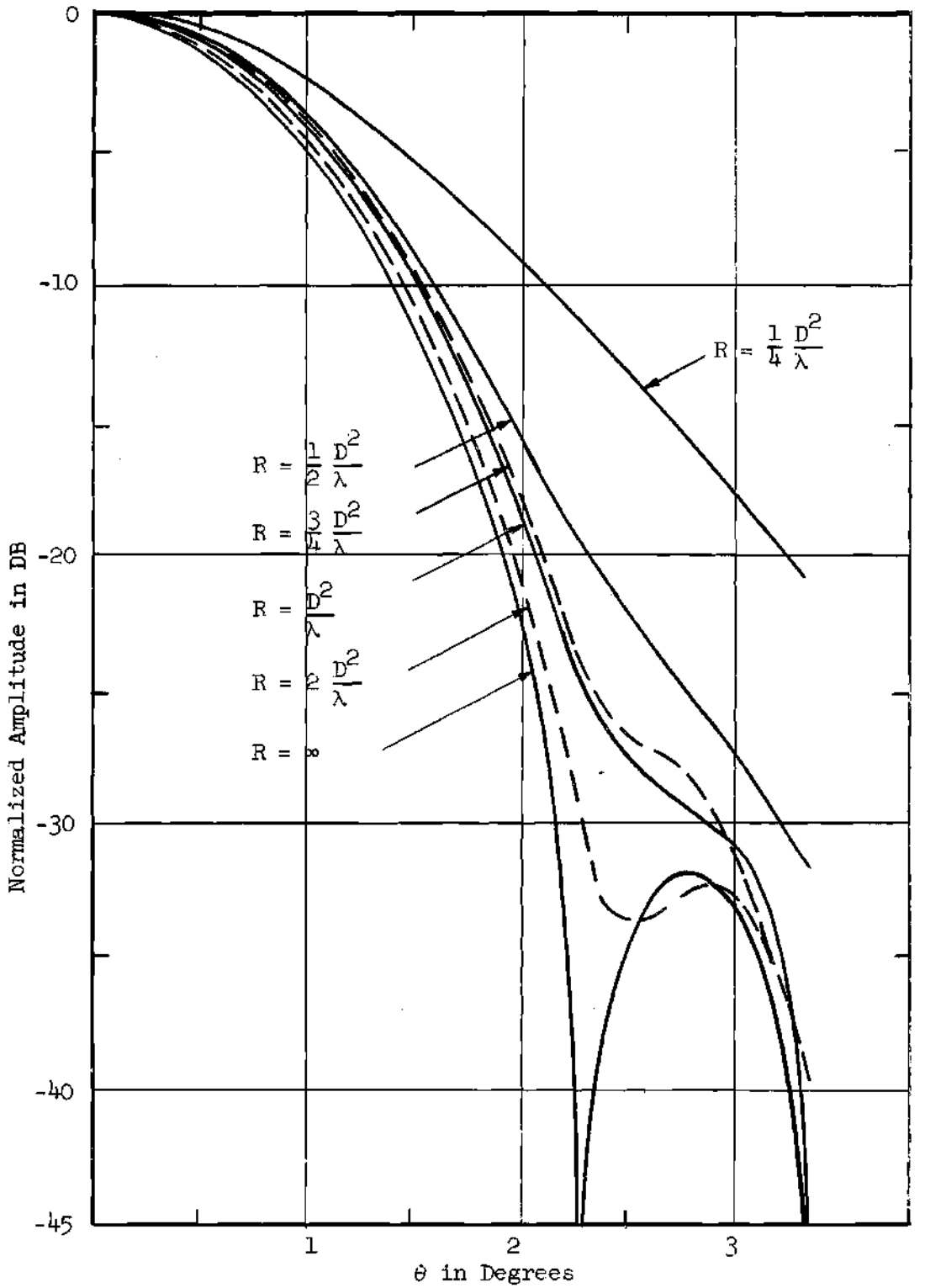

Figure 11. Radiation Patterns for Case Ic

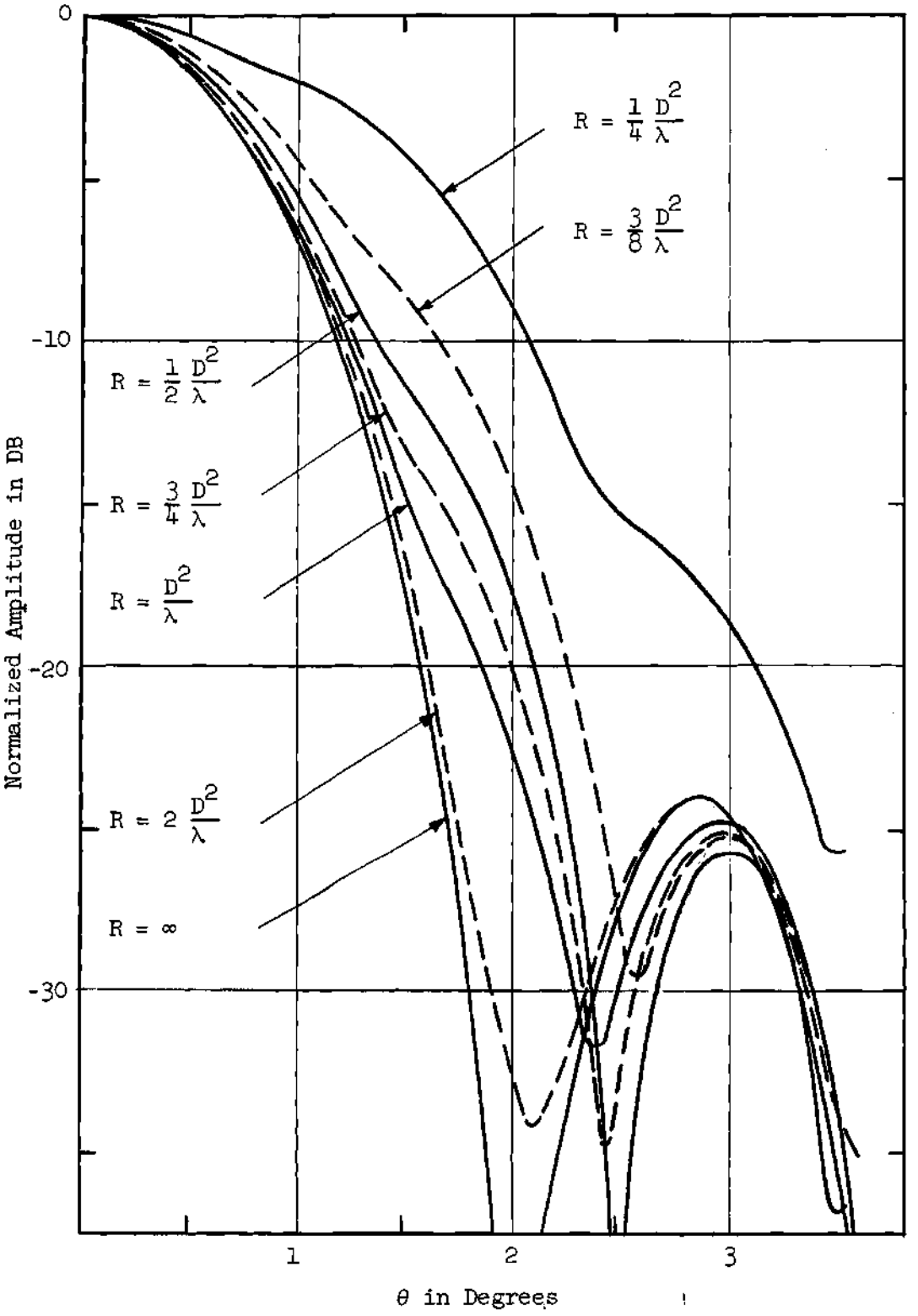

Figure 12. Radiation Patterns for Case Id

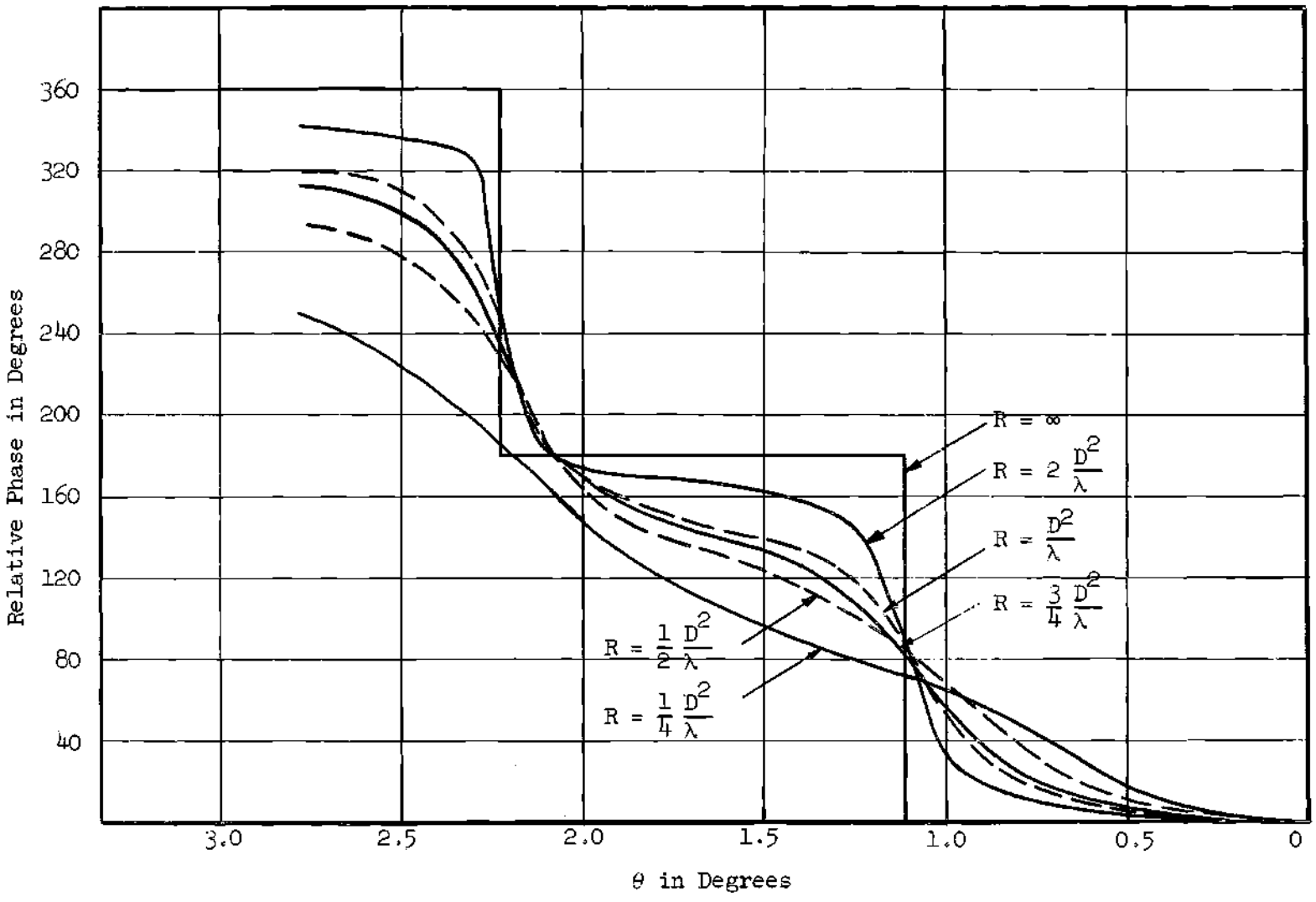

Figure 13. Phase Deviation for Case Ia

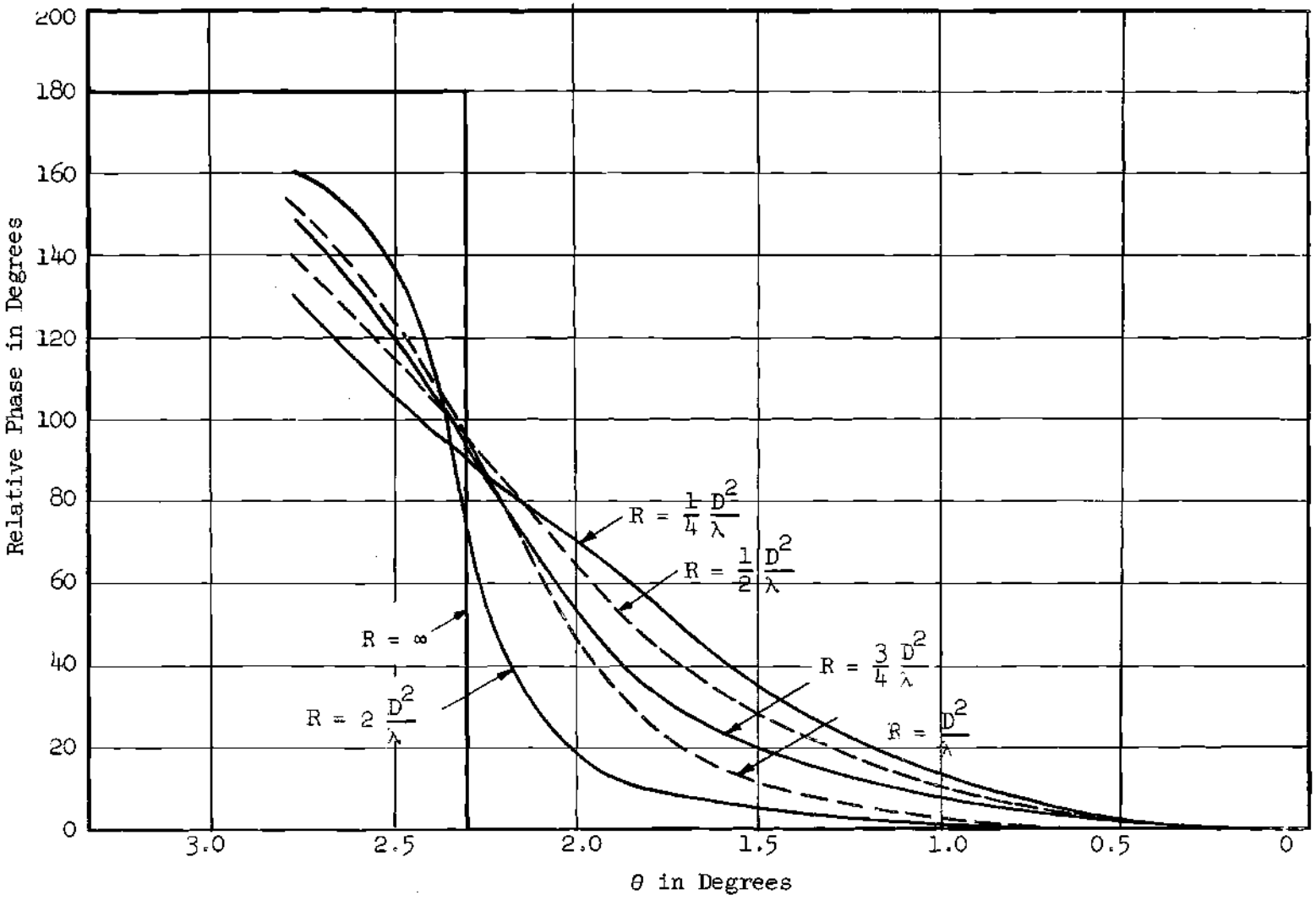

Figure 14. Phase Deviation for Case Ic

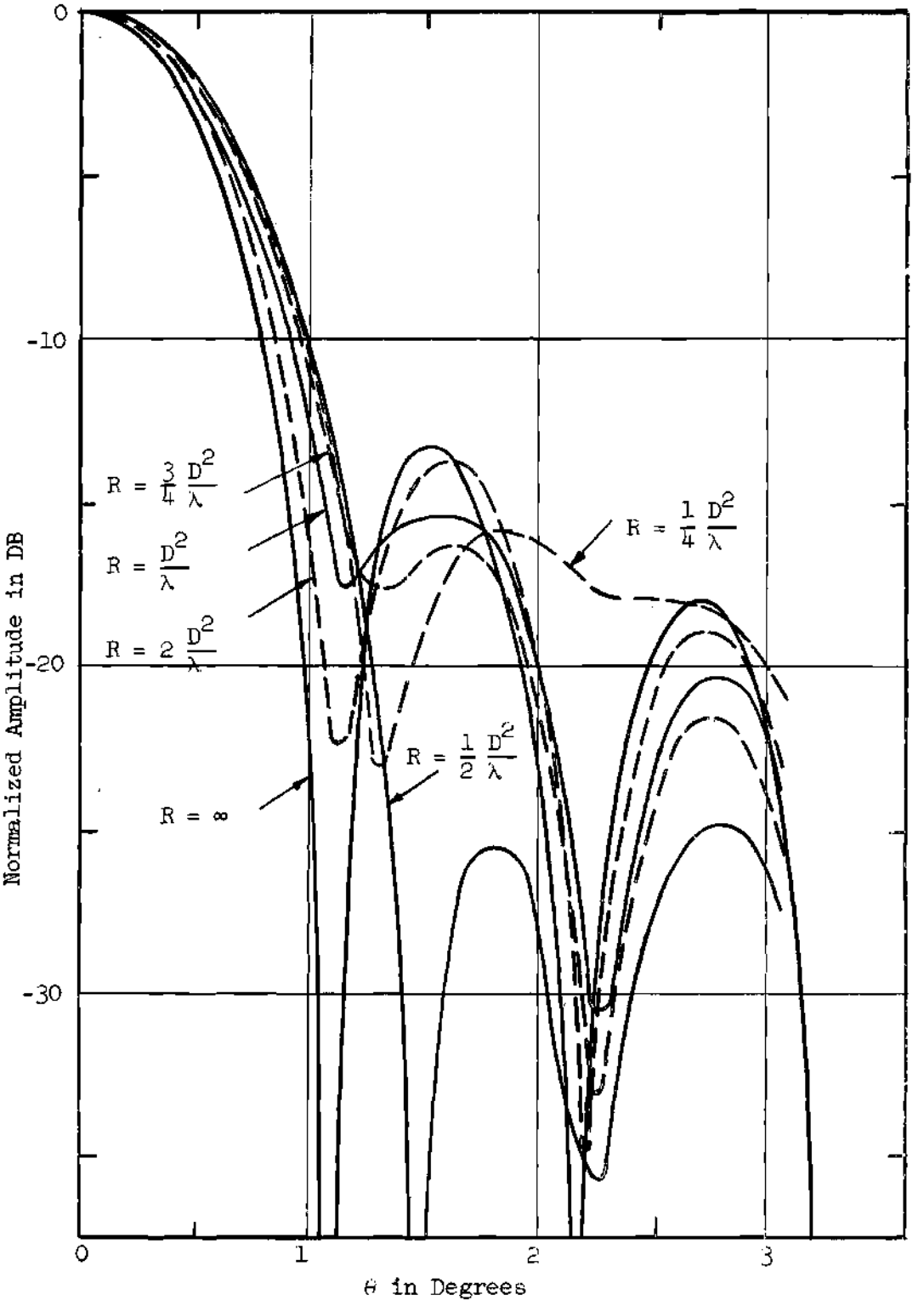

Figure 15. Radiation Patterns for Case IIa

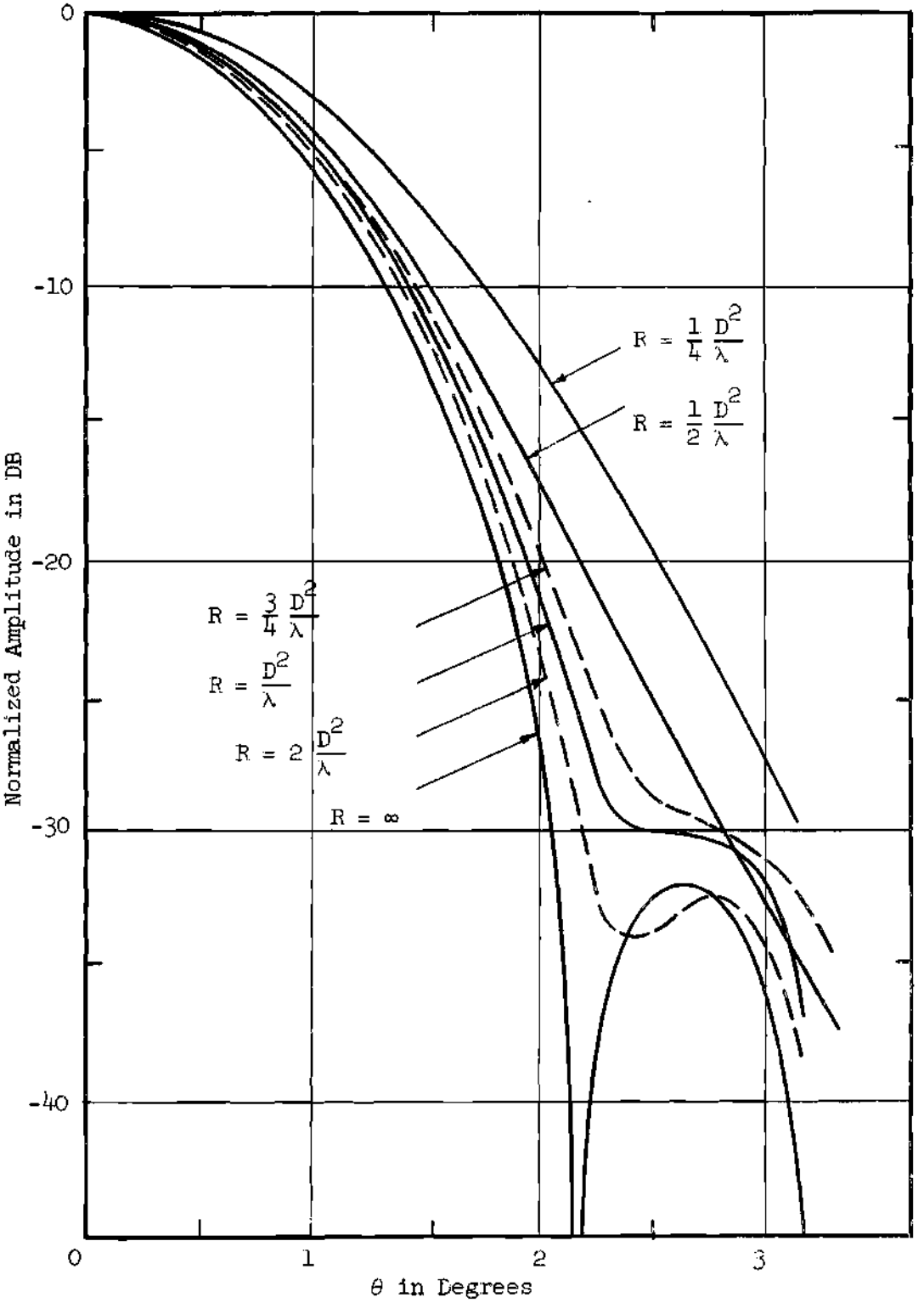

Figure 16. Radiation Patterns for Case IIc

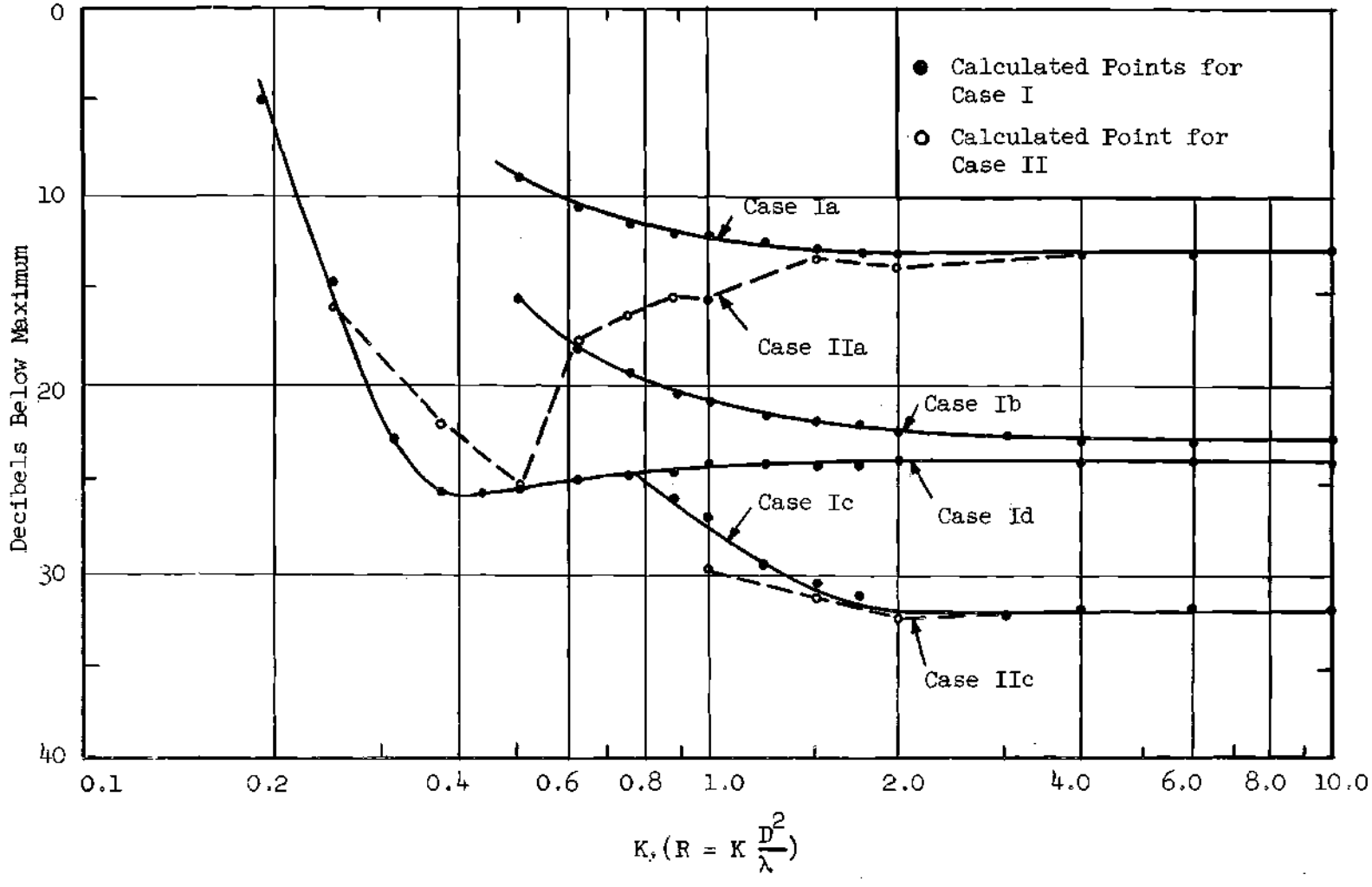

Figure 17. Variation of the First Sidelobe Level with Range for Case I and Case II

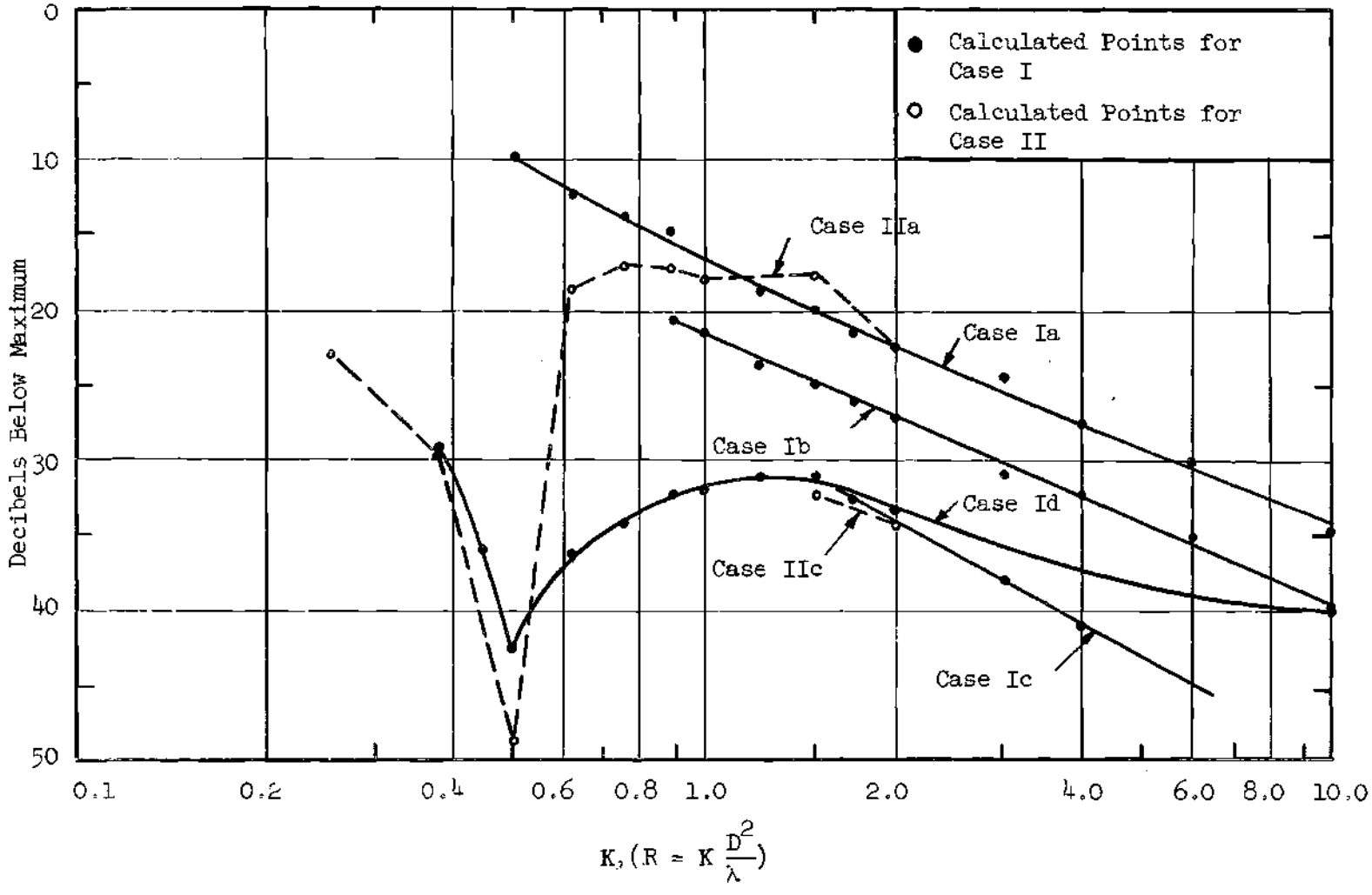

Figure 18. Variation of the First Null Depth with Range for Case I and Case II

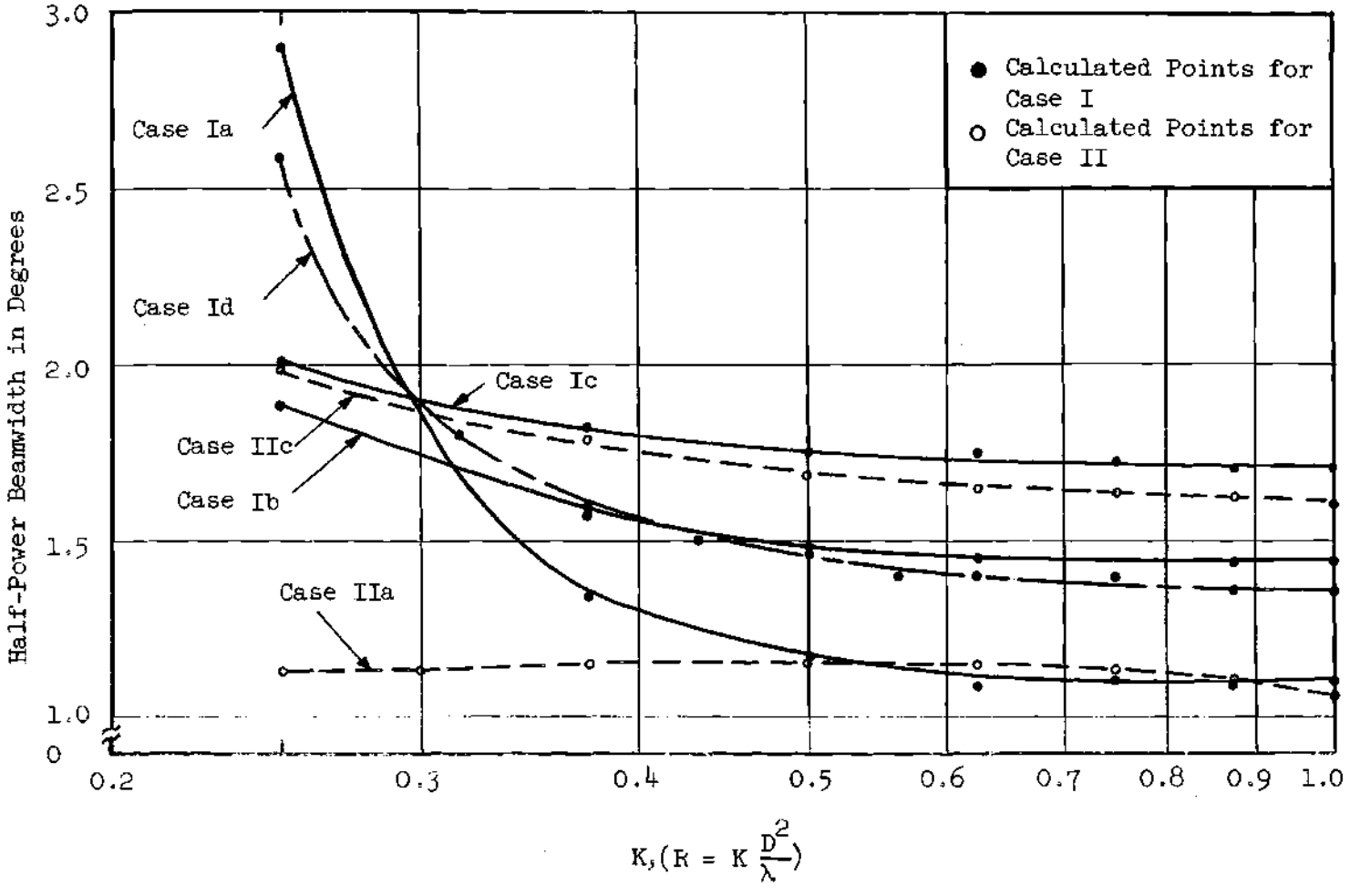

Figure 19. Variation of the Half-Power Beamwidth with Range for Case I and Case II

CHAPTER V

CONCLUSIONS AND DISCUSSION OF RESULTS

The summary curves shown in Figures 17, 18, and 19 show the level of the first sidelobe, the depth of the first null, and the half power beamwidth for Case I and Case II.

Case I, Point Source Illumination.--Some general conclusions may be drawn from the summary curves regarding the deterioration of the far field radiation pattern for the case of point source illumination. It may be generally said that as the distance to the point of observation is decreased, the main beam widens, and the sidelobes adjacent to the main beam are raised and finally swallowed into the main beam skirt. This can be clearly seen from Figures 9 through 12 of Chapter IV. It is also evident from these figures that for the more sharply tapered aperture functions, the sidelobes rise faster and blend into the main beam sooner as the point of observation is moved in toward the aperture. It may also be seen from these figures that the variation of half power beamwidth with range is reduced by increasing the taper of the amplitude function.

It will be noted, however, that the radiation patterns for the experimental aperture function, which was the only function not tapered to zero at the edge of the aperture, behaved in a somewhat different manner from the other three cases. Figures 17 and 18 show that the level of the first sidelobe and the level of the first null increased monotonically with decreasing distance for the three aperture functions which

were tapered to zero. The same characteristics plotted versus distance for the experimental aperture function exhibit a dip in their curves in the region of $R = D^2/2\lambda$. This condition is interesting and could be misleading since one usually assumes the far zone radiation pattern to have lower sidelobes and deeper nulls than the Fresnel pattern.

Using the experimental aperture function as an example, it is seen from Figures 17 through 19 that the first sidelobe level is within 1 db of its far zone value down to $R = D^2/\lambda$, and within 3 db of its far zone value down to $R = D^2/2\lambda$. On the other hand, it is shown that the first sidelobe level is within 3 db of its far zone value down to $R = D^2/\lambda$, and within 8 db of its far zone value down to $R = D^2/2\lambda$ for the $\cos(\pi/2x)$ aperture function. Variations between aperture functions are also observed for the half power beamwidths in Figure 19. It becomes apparent then that it is almost meaningless to talk about the Fresnel-far zone boundary of an antenna without considering its aperture field distribution. This points up the fact that the Fresnel zone patterns should be computed for each antenna in question to determine the minimum range R in which the far zone pattern may be reasonably represented.

Case II, Illumination by a Large Aperture Transmitter.--Since the primary objective of this thesis was to develop a technique for determining the radiation patterns in Case II, the following remarks are not meant to be characteristic of the general case of radiation patterns taken with large aperture transmitters. Radiation patterns are dependent to such a large degree on aperture size, aperture illumination function, and phase error, that there would exist an almost infinite

number of cases to completely describe the problem. However, some remarks can be made for the specific cases which were computed, and some conclusions can be drawn from this limited data.

The radiation patterns for Case IIc, $\cos^2(\pi/2x)$ aperture distribution, show very little change from Case Ic. This is true because of two compensating changes which occur in the aperture illumination function as the distance is decreased from the far zone to the Fresnel region. As the distance is decreased, the test antenna subtends more of the transmitting antenna's radiation pattern thus causing the amplitude distribution to deviate from its desired shape. This effect as shown in Figure 7 results in a tapering of the amplitude distribution. This tapering effect on the aperture amplitude function is counteracted by the phase deviation across the aperture which is less with a larger aperture transmitter than with a point source. This phase deviation reduction is shown in Table 1 which compares the maximum phase deviation as a function of range for Cases Ic and IIc. Thus as the distance to the point of observation is decreased, the tapering amplitude function tends to deteriorate the radiation pattern faster than for the case of point source illumination, while the decreasing phase deviation offsets this trend producing a net result of little or no change.

The results of Case IIa (uniform illumination) are not as easily compared to its counterpart, Case Ia. The first sidelobe and first null levels are no longer monotonically increasing functions with decreasing distance. Given a Fresnel radiation pattern for this case, it would be difficult indeed to say anything about what the far zone radiation

Table 1. Maximum Phase Deviation for Cases Ic and IIc

K ($R=KD^2/\lambda$)	Maximum Phase Deviation for Case Ic (Degrees)	Maximum Phase Deviation for Case IIc (Degrees)
∞	0	0
2	22.5	22.5
3/2	30.0	30.0
1	45.0	45.0
7/8	51.4	49.8
3/4	60.0	55.2
5/8	72.0	65.4
1/2	90.0	74.2
3/8	120.0	88.0
1/4	180.0	89.0

pattern would look like. An interesting observation is that the variation of the first sidelobe and first null with distance resembles that of Case Id which was the experimental aperture function. The dip in these curves once again occurs at $R = D^2/2\lambda$. It will be noticed from Figure 5 that the amplitude distribution for Case IIa at $R = D^2/2\lambda$ is very similar to the experimental aperture function shown in Figure 4.

The half power beamwidth for Case IIa is practically constant in the region $1/4\ D^2/\lambda < R < \infty$. This is contrary to what is expected, and points out that the Fresnel zone radiation patterns in this case can not be easily interpreted to obtain the true far zone radiation pattern. It may then be necessary in cases where antenna measurements must be made on ranges which are in the Fresnel zone of the test antenna and transmitting source to determine the far zone radiation pattern from a knowledge of what the Fresnel zone pattern should be under the existing conditions. This would mean that the aperture function of an antenna could be measured, and the Fresnel zone pattern determined for a given transmitting source by means of the technique set forth in this thesis. The Fresnel pattern so determined could be checked experimentally, and the far zone radiation pattern computed by means of the Fourier integral computer.

Recommendations.--It is the opinion of this author that more work on practical illumination functions which are not tapered to zero at the edge of the aperture would be beneficial. It has been shown in this thesis that general statements cannot be made concerning measurements in the Fresnel zone, and that each specific case must be computed to

determine what effect the measurements will have on the far zone radiation pattern. An experimental program would be useful in bearing out the applicability of this method to antenna measurements. Such a program would include the comparison of calculated and measured radiation patterns for different aperture field functions, and various size transmitting apertures.

APPENDIX I

DEFINITIONS OF FIELD TERMS

Far Field Region.--The far field region has two definitions. The first is based on radiation pattern distortion, and states that the far field region extends from a distance R in which the phase deviation from the center of the aperture to the edge does not exceed $\lambda/16$, to infinity. The far zone based on this definition is $2D^2/\lambda \leq R < \infty$. The second definition is based on axial power density. The far zone based on this definition is that region in which the axial power density varies as $1/R^2$, where R is the distance to the origin of the aperture surface. This condition is fulfilled for $D^2/\lambda \leq R < \infty$.

Fresnel Region.--The Fresnel region extends from a distance of several aperture diameters to D^2/λ or $2D^2/\lambda$ depending on your definition of the far zone and the approximations used in the exact equations. The Fresnel field is a $1/r$ field in aperture coordinates but requires many terms of the form $1/R^n$ in space coordinates.

Near Field Region.--That region from the aperture surface to the Fresnel region. The near field requires many terms in the form $1/r^n$ both in aperture and space coordinates.

APPENDIX II

DERIVATION OF THE RELATIONS BETWEEN THE APERTURE FIELD AND THE FRESNEL FIELD

The electromagnetic field at any point P in the right hemisphere, due to diffraction through a large plane aperture of arbitrary shape and size situated in the x-y plane, may be described by the following equation (6) (see Figure 1).

$$\bar{A}(\theta,\phi) = \frac{1}{4\pi}\int_S F(x,y)e^{j\Psi(x,y)}\,\frac{e}{r}^{-jKr}\,[(jK + \frac{1}{r})\bar{i_z}\cdot\bar{r} + jK\bar{i_z}\cdot\bar{s}]dxdy \qquad (28)$$

where

$F(x,y)e^{j\Psi(x,y)} = \bar{F}(x,y)$ is the amplitude and phase distribution of the electromagnetic field over the surface of the aperture,

λ is the wavelength of the radiated field,

K is $2\pi/\lambda$,

$\bar{s}$, $\bar{i_z}$, $\bar{r}$ are unit vectors, $\bar{s}$ being a unit vector in the direction of power flow at the surface of the aperture, and $\bar{i_z}$ and $\bar{r}$ being described in Fig. 1.

This equation describes the field only if the effect of the line integrals around the edge of the aperture are ignored, and the field

across the aperture is linearly polarized. A solution of the near field using Equation (1) can at best give only qualitative results since the line integrals make significant contributions to the field in this region.

In the Fresnel and far zones certain simplifying approximations can be made which greatly reduce the complexity of Equation (1). These approximations will be investigated for an aperture of width $D = 50\lambda$, and a minimum range $R = 1/4\ D^2/\lambda$. The reduction of Equation (1) to the narrow beam Fresnel and far zone equations will follow the procedure outlined by Silver (8).

As the distance from the point of observation to the aperture surface increases, we pass from the near zone into the Fresnel zone. Several simplifying approximations may be introduced in this region. First, the term $1/r$ in the brackets of Equation (1) becomes negligible with respect to K. The term $\overline{i_z}\cdot\overline{r}$ is considered constant over the aperture surface and is set equal to $\overline{i_z}\cdot\overline{R} = \cos\theta$, where $\overline{R}$ is the radius vector from the center of the aperture to P. We may also consider that the variation of the term $1/r$ outside the brackets may be ignored, and the term may be replaced by the reciprocal distance $1/R$ from the field point P to the origin.

To illustrate the validity of these approximations as applied to the computations made in this thesis, consider an aperture of width $D = 50\lambda$. Then, $R_{min} = D^2/4\lambda = 625\lambda$, and $K = 2\pi/\lambda \gg 1/r = 1/625\lambda$. For a narrow beam antenna, whose halfpower beamwidth is less than 30°, r_{max} is given approximately by (see Fig. 1)

$$r_{max} \cong \frac{50\lambda}{\sin\left[\tan^{-1}\left(\frac{50\lambda}{625\lambda}\right)\right]} \cong 625.7\lambda \tag{29}$$

We may then reason that negligible error results in the use of 1/R for the term 1/r outside the brackets, and the use of $\overline{i_z}\cdot\overline{R} = \cos\theta$ for $\overline{i_z}\cdot\overline{r}$ inside the brackets.

The variation of r over the aperture surface must be examined more carefully in the phase term e^{-jKr}. In general, we may write

$$r = [(x_1 - x)^2 + (y_1 - y)^2 + z^2]^{1/2} \tag{30}$$

where

$(x, y, 0)$ are the coordinates of a point on the aperture surface,

and (x_1, y_1, z) are the coordinates of a point P in the right hemisphere.

If the point P is sufficiently far from the aperture surface, such that $z \gg |x_1-x|,\ |y_1-y|$, then

$$r \approx z + \frac{(x_1-x)^2}{2z} + \frac{(y_1-y)^2}{2z} + \ldots . \tag{31}$$

Now let

$$\begin{aligned} x_1 &= R \sin\theta \cos\phi \ , \\ y_1 &= R \sin\theta \sin\phi \ , \\ z &= R \cos\theta \ , \end{aligned} \tag{32}$$

and we have

$$r \approx R\cos\theta + \frac{(R\sin\theta\cos\phi - x)^2}{2R\cos\theta} + \frac{(R\sin\theta\sin\phi - y)^2}{2R\cos\theta} + \ldots \quad (33)$$

If $\frac{x\sin\theta\cos\phi}{R} \ll 1$, $\frac{y\sin\theta\sin\phi}{R} \ll 1$, then all terms of order higher than the second may be neglected, and

$$r \approx R - (x\sin\theta\cos\phi + y\sin\theta\sin\phi) + \frac{x^2 + y^2 - (x\sin\theta\cos\phi + y\sin\theta\sin\phi)^2}{2R} \quad . \quad (34)$$

Examining the terms $\frac{x\sin\theta\cos\phi}{R}$, and $\frac{y\sin\theta\sin\phi}{R}$ we will consider

$$\begin{aligned} x_{max} &= 50\lambda \ , \\ y_{max} &= 50\lambda \ , \end{aligned} \quad (35)$$

$$|\sin\theta|_{max} = |\cos\phi|_{max} = |\sin\phi|_{max} = 1$$

then

$$\left|\frac{x\sin\theta\cos\phi}{R}\right|_{max} = \left|\frac{y\sin\theta\sin\phi}{R}\right|_{max} \leq \frac{x_{max}}{R} = \frac{y_{max}}{R} \leq \frac{50\lambda}{625\lambda} \leq .08 \quad (36)$$

Hence, it is reasonable to use the approximation that

$$e^{-jKr} = e^{-jK\left[R-(x\sin\theta\cos\phi+y\sin\theta\sin\phi) + \frac{x^2+y^2 - (x\sin\theta\cos\phi+y\sin\theta\sin\phi)^2}{2R}\right]} \quad (37)$$

Now, if we let

$$\sin\theta\cos\phi = \alpha \ ,$$

$$\sin\theta\sin\phi = \beta \ ,$$

the Fresnel approximation to Equation (1) becomes

$$\bar{A}(\theta) = \frac{je^{-jKR}}{2\lambda R}\int_s \bar{F}(x,y)e^{-jK\left[(x\alpha+y\beta) - \frac{x^2-y^2+(x\alpha+y\beta)^2}{2R}\right]}$$

$$[\cos\theta + \bar{i}_z\cdot\bar{s}]dxdy \ . \qquad (38)$$

It has been shown by Plonsey (8) that the limit of validity of Equation (38) is $|\theta| > 30°$.

Equation (38) may be further simplified if all the energy is concentrated in a narrow angular region about the z axis. The half-power beamwidths used in the computation of radiation patterns in Chapter IV ranged from 1.06° for uniform illumination to 1.71° for $\cos^2(\frac{\pi}{2}x)$ illumination. Since the variation of $\cos\theta$ over this range is negligible, we would be justified in setting $\cos\theta$ equal to its maximum value of unity. If the phase deviation across the aperture is small, we may also set $\bar{i}_z\cdot\bar{s}$ equal to unity, and Equation (38) may be written

$$\bar{A}(\theta) = \frac{je^{-jKR}}{\lambda R}\int_s \bar{F}(x,y)e^{-jK\left[(x\alpha+y\beta) - \frac{x^2-y^2+(x\alpha+y\beta)^2}{2R}\right]}dxdy \qquad (39)$$

It was shown in Chapter III that for point source illumination, a phase deviation of $e^{-j\frac{Kx^2}{2R}}$ appears across the aperture surface. If the phase deviation is sufficiently large, the term $\bar{i}_z\cdot\bar{s} = \cos\gamma$ can no

longer be set equal to unit across the aperture surface. It can be shown that

$$\gamma = \tan^{-1}\left[\frac{\partial\Psi(x)}{\partial x}\cdot\frac{1}{K}\right] , \tag{40}$$

and for $\Psi(x) = \frac{Kx^2}{2R}$, $\gamma = \tan^{-1} x/R$. The maximum phase deviation occurs at the minimum range distance, and we may write

$$\gamma_{max} = \tan^{-1}\frac{D/2}{R_{min}} = \tan^{-1}\frac{25\lambda}{625\lambda} = 2.30^\circ .$$

The maximum range of the cos γ term then is $.99919 \leq \cos\gamma \leq 1$, and the deviation in cos γ may be neglected.

Equation (39) may be reduced to a two-dimensional form for exploration in a given plane by methods outlined by Silver (9). If this is done, these equations take on the form

$$\bar{A}(\theta) = \frac{je^{-jKR}}{\lambda R}\int_{-a}^{a}\bar{f}(x)e^{-jK\left[x\sin\theta + \frac{x^2(\sin^2\theta-1)}{2R}\right]}dx \tag{41}$$

for exploration in the x-z plane. If θ is very small, $\sin^2\theta \ll 1$, the narrow beam Fresnel equation may be written as

$$\bar{A}(\theta) = \frac{je^{-jKR}}{\lambda R}\int_{-D/2}^{D/2}\bar{f}(x)e^{-jK\left[x\sin\theta - \frac{x^2}{2R}\right]}dx \tag{42}$$

where

$$\bar{f}(x) = \int_{-b}^{b}\bar{F}(x,y)dy , \tag{43}$$

(see Fig. 1).

In the far zone, where $R > 2D^2/\lambda$, Equation (42) may be further reduced to

$$\bar{A}(\theta) = \frac{je^{-jKR}}{\lambda R}\int_{-a}^{a} \bar{f}(x)e^{-jK\sin\theta x}\,dx\,, \tag{44}$$

or

$$\bar{A}(v) = c\int_{-a}^{a} \bar{f}(x)e^{-jvx}\,dx \tag{45}$$

where

$$c \quad \text{is} \quad \frac{je^{-jKR}}{\lambda R}\,,$$

and

$$v \quad \text{is} \quad K\sin\theta.$$

APPENDIX III

THE FOURIER INTEGRAL COMPUTER

The computer used in the calculation of the radiation patterns for this thesis was the Scientific-Atlanta Model CFI Fourier Integral Computer. This computer used along with the Scientific-Atlanta Model APR-20 Pattern Recorder automatically evaluates the integral

$$\bar{I}(u) = \int_{-1}^{1} \bar{P}(x) e^{jux} dx \ , \tag{46}$$

and records the absolute magnitude of $\bar{I}(u)$ on the pattern recorder as a function of the parameter u.

The simplified block diagram in Figure 20 shows how the integral is evaluated by the computer. The amplitude function P(x), and the phase function $\Psi(x)$ are drawn in pencil or ink on a special dual graph paper. The curves are normalized and may assume any shape with the exception that they must be single valued with respect to x.

The peak magnitudes of the two functions are set in on two separate potentiometers. The phase function potentiometer allows a range of 0 to 30π radians for Ψ. The curves are clipped to the drum of a graph-reading function generator with the x-axis parallel to the drum axis. As the drum rotates at 4580 rpm, two synchronized photoelectric heads scan the curves along the x-axis. In every drum revolution,

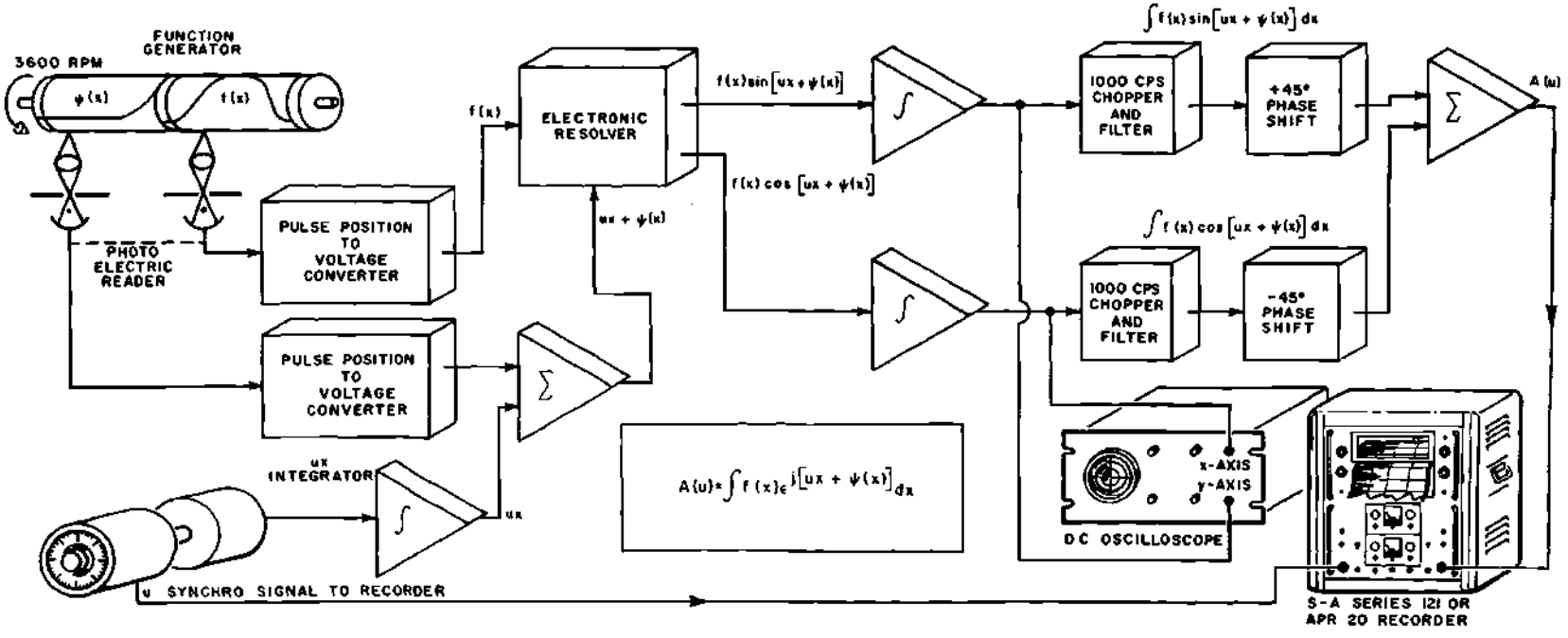

Figure 20. Simplified Block Diagram of Model CF 1 Fourier Integral Computer.

passage of each curve under its phototube generates a pulse whose time position is a measure of the function magnitude. Two pulse position-to-voltage converters generate varying direct voltages whose waveforms are reproductions of the amplitude and phase curves drawn on the graphs. A complete traverse of the X-axis is made in four seconds, so that each function is sampled at 305 points.

The phase argument of the integrand in Equation 46 is the sum of the phase function $\Psi(x)$ and the product ux. A precision 10-turn helical potentiometer develops a voltage proportional to the parameter u. The voltage is then integrated to produce a linear voltage ramp with instantaneous amplitude proportional to ux. A summation circuit produces the total phase argument $\Psi(x) + ux$. A synchro transmitter and a motor are geared to the u potentiometer. The synchro transmitter controls the chart position of a Scientific-Atlanta antenna pattern recorder. The motor automatically advances u after each integration period.

An electronic resolver performs the conversion:

$$P(x)e^{j[\Psi(x) + ux]} = P(x) \cos [\Psi(x) + ux] + jP(x) \sin [\Psi(x) + ux] \quad (2)$$

The resolver is capable of operation through 30 revolutions of $\Psi(x) + ux$. The two quadrature components of the integrand are applied to chopper-stabilized electronic integrators which evaluate corresponding components of the integral between the x limits of -1 and 1. A complex-plane plot of the integral is displayed by means of a long-persistence oscilloscope. The display provides a means of reading the phase of the solution and is useful in studying the generation of the solution. After integration,

the quadrature signals are converted to 1-kc sine-wave voltages which are added in phase quadrature to provide an output proportional to I(u).

Recording the solution, resetting the integrators, and advancing the parameter u are accomplished automatically during the retrace of the scanning heads in the function generator. In addition, chopper-stabilized "memory" circuits automatically zero-set the function generator and resolver to eliminate the manual adjustments ordinarily required in similar analog devices.

Each integration cycle establishes one point of the solution. Repetitive integration and u advance generate a 250-point solution in about 35 minutes.

The accuracy of the function generator used in the Model CF 1 computer is within 1% of x, P(x), or Ψ(x). The static pen position accuracy for the Model APR-20 pattern recorder in the logarithmic mode is better than $\pm$ 0.5 of full scale over the first 20 db and better than $\pm$ 1% over the next 20 db. It has been shown by Wynn (10) that the overall accuracy of the two instruments is $\pm$ 0.25 db for 0 to 10 db, $\pm$ 0.5 db for 10 to 20 db., $\pm$ 1.0 db for 20 to 30 db, $\pm$ 2 db for 30 to 35 db, and $\pm$ 3 db for 35 to 40 db.

BIBLIOGRAPHY

Literature Cited:

1. Silver, S., Microwave Antenna Theory and Design, New York, McGraw-Hill Book Company, Inc., 1949, pp. 158-174.

2. Bickmore, R. W., "Fraunhofer Pattern Measurements in the Fresnel Region," Canadian Journal of Physics, Volume 35, No. 11, November 1957, pp. 1299-1308.

3. Hansen, R. C., and Bailin, L. L., "New Method of Near Field Analysis," Institute of Radio Engineers Transactions on Antennas and Propagation, Volume AP-7, December 1959, pp. 5458-5467.

4. Hu, M. K., Study of Near-Zone Fields of Large Aperture Antennas, Syracuse University Research Institute, Syracuse, New York, Final Report, Part 2, RADC-TR-57-126B, April 1957.

5. Polk, C., "Optical Fresnel-Zone Gain of a Rectangular Aperture," Institute of Radio Engineers Transactions on Antennas and Propagation, Volume AP-4, No. 1, January 1956, pp. 65-69.

6. Silver, Op. Cit., p. 166.

7. Ibid., pp. 169-173.

8. Plonsey, R., "Aperture Fields," Institute of Radio Engineers Transactions on Antennas and Propagation, Volume AP-9, No. 6, November 1961.

9. Silver, Op. Cit., pp. 182-185.

10. Wynn, W. D., The Effect of Common Predictable Surface Errors on the Radiation Pattern of a Paraboloid, Unpublished M.S. Thesis, Georgia Institute of Technology, 1961.

Other References:

1. Cheng, D. K., Phase-Error Effect in Microwave Antennas, Syracuse University Research Institute, Syracuse, New York, Interim Report on Contract Nos. AF 30(120)-425-E.E. 4, and AF 30(602)-300, April 1952 and September 1953.

2. Kraus, J. D., Antennas, New York, McGraw-Hill Book Company, Inc., 1950.

3. Moseley, R. E., Shaping Microwave Antenna Radiation Patterns by an Aperture-Field Method, Unpublished M.S. Thesis, Georgia Institute of Technology, 1959.